

NEW X-RAY CLUSTERS IN THE *EINSTEIN* EXTENDED MEDIUM SENSITIVITY SURVEY I: MODIFICATIONS TO THE X-RAY LUMINOSITY FUNCTION

AARON D. LEWIS^{1,2,3}, JOHN T. STOCKE^{1,2}, E. ELLINGSON^{1,2}

Center for Astrophysics and Space Astronomy, University of Colorado, 389 UCB, Boulder, CO 80309

AND

ERIC J. GAIDOS⁴

Center for Space Research, Massachusetts Institute of Technology, Cambridge, MA 02139

Received 2000 November 1; accepted 2001 August 29

ABSTRACT

The complete ensemble of *Einstein* Imaging Proportional Counter (IPC) X-ray images has been re-processed and re-analyzed using a multi-aperture source detection algorithm. A catalog of 772 new source candidates detected within the 38 arcmin diameter central regions of the 1435 IPC fields comprising the Extended Medium Sensitivity Survey (EMSS) has been compiled. By comparison, 478 EMSS sources fall within the same area of sky. A randomly-selected subsample of 133 fields was examined; 73 sources were detected and compared with 49 original EMSS sources in the same region of sky. We expect, based on confusion statistics, that most of these sources are either the summation of two or more lower count rate point sources that fall within the larger detection apertures or are single point sources. An optical imaging study discovered one possible cluster of galaxies among 43 identified sources, suggesting that $\leq 2.3\%$ of the full catalog of sources are extrapolated to be actual distant ($z \geq 0.14$) clusters whose extended X-ray structure kept them from being detected in the EMSS despite having sufficient total flux.

We have constructed other subsamples specifically selected to contain those X-ray sources most likely to be clusters based upon additional X-ray and optical criteria. Both a database search and an optical imaging study of these subsamples have found several new distant clusters, setting a firm lower limit on the number of new clusters in the entire catalog. Given both the numbers of new EMSS clusters and their spectroscopic or photometric redshifts, we estimate that the original EMSS cluster sample is 72 – 83% complete. We update the Henry et al. (1992) EMSS distant ($z \geq 0.14$) cluster sample with more recent information, and use the redshifts and X-ray luminosities for these new EMSS clusters to compute revised X-ray Luminosity Functions (XLFs) in the three redshift shells defined by Henry et al. (1992). The addition of these new high- z , high- L_X clusters to the EMSS is sufficient to remove the requirement for “negative” evolution at high- L_X out to $z \sim 0.5$. Although the best estimate of the EMSS XLF at $z = 0.3 - 0.6$ and $\log L_X$ of 44.9 – 45.2 ergs s⁻¹ falls 1σ below the low- z (< 0.3) XLF, the optical identification of the full 772 source catalog remains incomplete. We conclude that the EMSS has systematically missed clusters of low surface brightness. Since all X-ray cluster surveys are less sensitive to low surface brightness emission, they may be also be affected.

Subject headings: surveys — galaxies: clusters: general — X-rays: general

1. INTRODUCTION

The *Einstein* Extended Medium Sensitivity Survey (EMSS) of X-ray sources was constructed from serendipitous detections in Imaging Proportional Counter (IPC) images at high Galactic latitude free of very bright or extended target sources (Gioia et al. 1990b). This catalog has served as the foundation for investigations of the statistical properties of several different classes of objects, including stars, active galactic nuclei (AGN), BL Lac objects, and clusters of galaxies (Stocke et al. 1991; Gioia & Luppino 1994). The sample of EMSS X-ray clusters is of special cosmological interest since these objects can be de-

tected to high redshift and, because of the density-squared dependence of the X-ray emission and the low volume filling factor ($\sim 10^{-7}$) of X-ray luminous clusters, X-ray-selected samples are not significantly affected by the confusion and projection effects which plague optically-selected catalogs. Thus X-ray cluster surveys are potentially powerful tests of cosmology and structure formation models (e.g., Eke et al. 1996; Donahue et al. 1998; Bahcall & Fan 1998; Donahue & Voit 1999). Our knowledge of X-ray cluster statistics and evolution has dramatically increased with the advent of large solid-angle, high-sensitivity X-ray surveys such as the EMSS (Gioia et al. 1990b; Henry et al. 1992, H92 hereafter), the *ROSAT* All Sky Survey (RASS,

¹ lewisa@uci.edu, stocke@casa.colorado.edu, e.elling@casa.colorado.edu

² Visiting Astronomer, Kitt Peak National Observatory, National Optical Astronomy Observatories, which is operated by the Association of Universities for Research in Astronomy, Inc. (AURA) under cooperative agreement with the National Science Foundation.

³ Current Address: University of California, Irvine, Department of Physics and Astronomy, 4171 Frederick Reines Hall, Irvine, CA, 92697-4575

⁴ Current Address: Division of Geology and Planetary Science, California Institute of Technology 170-25, Pasadena, CA 91125, gaidos@gps.caltech.edu

Truemper 1993; Ebeling et al. 1996, 2001; de Grandi et al. 1999; Moscardini et al. 2000), as well as the investigation of the deepest regions of the RASS, the North Ecliptic Pole Survey (NEP, Gioia et al. 2001), and collections of serendipitous sources found in deeper *ROSAT* pointed observations (Rosati et al. 1995; Scharf et al. 1997; Vikhlinin et al. 1998a; Romer et al. 2000; Perlman et al. 2000).

The interpretation of these surveys as tests of cosmological models must include various theoretical effects, the most pronounced of which may be the thermal history of the X-ray-emitting gas (Evrard & Henry 1991; Kaiser 1991). In addition, there may be systematic errors introduced by the methods used to analyze the X-ray imaging data. The possibility that past X-ray source catalogs developed from *Einstein* IPC images suffer from bias or incompleteness motivated re-analyses of the data (Hamilton & Helfand 1993; Moran et al. 1996; Oppenheimer et al. 1997, OHG97 hereafter). Although the *Einstein* data have been surpassed by the increased sensitivity and larger field of view of the *ROSAT* Position Sensitive Proportional Counter (PSPC), the EMSS catalog remains one of the largest sky-area sample of X-ray clusters against which others are compared. Due its large areal coverage, it is the only published survey to explore the highest luminosity region of the cluster X-ray Luminosity Function (XLF), in which the greatest leverage is obtained for constraining evolution in the XLF. Further, the EMSS catalog is one of the few large-sky-area source catalogs which has been thoroughly investigated and almost completely identified optically regardless of inferred source character; e.g., some of the deep *ROSAT* cluster searches have used algorithms to select only extended X-ray emitters, which are therefore the only sources investigated optically (c.f., Gioia et al. 2001). Additionally, accurate X-ray temperatures of high- z EMSS clusters obtained by *ASCA* (Henry 1997; Donahue et al. 1998, 1999) have allowed significant constraints to be placed on the value of Ω_{matter} (Bahcall & Fan 1998; Donahue & Voit 1999; Voit 2000; Henry 2000). With such a wealth of unique data now available for the EMSS sample, re-visiting the IPC data is still warranted.

New work on the IPC imaging data is characterized by two advancements. First, the IPC response flat-fielding, temporal event filtering, and exposure maps have been improved, reducing systematic errors that limit source detection (for detailed discussion, see OHG97). Second, a more sophisticated algorithm for source detection has been implemented. Previous IPC source catalogs such as the EMSS were constructed using a single 2.4 arcmin square detection aperture whose size was optimized for the detection of point sources. Thus such a catalog is biased towards point sources or sources with a high central surface brightness. While such a catalog may be complete to a certain X-ray flux *within the detection cell*, more extended sources with integrated fluxes above the survey threshold levels may have been excluded due to their lack of concentrated emission. Since X-ray clusters are often resolved in imaging data, this bias could significantly affect their apparent statistics in the catalog. Pesce et al. (1990) noted that up to 75% of the clusters in the original *Einstein* Medium Sensitivity Survey would have been excluded had they lacked centrally-peaked X-ray emission. But it is now known from *ROSAT* imaging that not all EMSS clus-

ters are so centrally-peaked as to suggest “cooling flows” (e.g., Donahue et al. 1992; Lewis et al. 1999) and some are quite diffuse as X-ray emitters (e.g., MS 1621.4+2146; Morris et al. 1998). Using simple models of the X-ray surface-brightness distribution of clusters, H92 and Donahue et al. (1992) estimated that the fraction of emission of a typical EMSS cluster falling outside the 2.4 arcmin square detection cell was between 38 and 93%, with a median value of 58%. For this reason, the XLF analysis by Gioia et al. (1990a) and H92 used only EMSS clusters at $z \geq 0.14$, where the percentage of the total flux falling outside the detect cell was not prohibitively large. Furthermore, nearby ($z \leq 0.14$) clusters were frequently the targets of the IPC observations, and were therefore unavailable to the EMSS as serendipitous sources.

This work addresses the question of whether there are a significant number of previously undetected serendipitous sources which fall in the EMSS fields and have count rates sufficiently high to justify inclusion in the EMSS catalog, but which have been previously excluded due to systematic errors or biases in the construction of that catalog. OHG97 constructed an X-ray source catalog from a complete database of archived IPC images using a detection algorithm that employed multiple apertures of different sizes to minimize X-ray surface-brightness selection effects. Several thousand new unidentified sources were found, of which more than 300 appear to be significantly extended. The OHG97 IPC source catalog is used as the starting point for this investigation, but several important observational details in the selection process must be considered herein in order to match the EMSS selection as accurately as possible, excepting detection aperture. While OHG97 eventually selected sources based on angular extent, all potential sources within the EMSS fields are considered here.

In §2 the OHG97 catalog construction method is summarized and the sources scrutinized to determine if each would have been included in the EMSS, in an attempt to make a truly flux-limited catalog. In §3 the nature of these “new” X-ray sources is investigated using available databases and optical observations of a randomly-selected subsample of these new sources. Since very few new distant clusters were found in the random sample, in §4 we investigate two non-random subsamples of sources specifically selected to maximize the discovery of distant clusters. Using the results from these subsamples, the source catalog is finalized in §5 for the most accurate comparison with the EMSS as possible; i.e., a sample whose selection matches the EMSS selection process as accurately as possible, given the different methods. The statistical effect of these new sources on the EMSS XLF results is also estimated in §5. A summary and conclusions are presented in §6. We assume $H_0 = 50h_{50}^{-1} \text{ km s}^{-1} \text{ Mpc}^{-1}$, $\Omega_0 = 1.0$, and $\Lambda = 0$, unless otherwise stated.

2. CONSTRUCTION OF THE NEW SOURCE CATALOG

The Imaging Proportional Counter (IPC) was one of the primary instruments on the High Energy Astrophysical Observatory (HEAO)-2 *Einstein* satellite which operated for two and a half years beginning in November 1978 (Giacconi et al. 1979). The IPC was an imaging proportional counter and the X-ray telescope/detector combination was

sensitive to photons in the energy range 0.2 to 4.0 keV with an effective area of about 100 cm². The field of view was 76 arcmin on a side with an on-axis resolution of 1.5 arcmin. During its operation, the IPC obtained nearly 4100 images with exposure times ranging from 100-56,000 seconds. The celestial coordinates of every photon detected in IPC images are recorded on optical disk archives at the Columbia University Center for Astrophysics. This merged image database was used to construct a new IPC source catalog independent of the EMSS. The *Einstein* data products were also processed by the CfA at Harvard, and are available through the HEASARC service⁵.

2.1. Source Detection

The source detection process has been described in detail in Hamilton et al. (1991), Moran et al. (1996) and OHG97. Here, only the essential elements of the algorithm are reviewed. Briefly, the distinctions between our procedures and the standard *Einstein* processing system include the application of a flat field to compensate for IPC detector nonuniformities, improved data editing, a circular (rather than square) source aperture, a local background determination for each search cell, and an iterative source search algorithm using apertures of different sizes.

The preliminary source catalog was constructed using only the unobstructed 38 × 38 arcmin center of the IPC field of view. Cumulative IPC event lists, exposure maps, and energy-dependent flat fields were constructed for each spacecraft orbit, with restrictions on allowable energy channels and telescope-Sun angles. The computed count rates in the 0.3 – 3.5 keV bandpass for all orbits were then summed into cumulative count and count-rate maps with 32 or 64 arc-second pixels. The maps were scanned with a series of four circular apertures with different diameters: 2.5, 4.7, 8.4, and 12.2 arcmin (alternatively, we will refer to these as the 1st, 2nd, 3rd, and 4th apertures, respectively). The smallest aperture is the optimal size for the detection of point sources and has 85% of the sky area of the 2.4 arcmin square detect cell aperture of the EMSS. The size of the largest aperture is limited by the field of view. Subsequent analysis showed that, for the 12.2 arcmin aperture, flat-fielding and vignetting corrections are too large and source confusion too frequent to make detections in that aperture viable. Therefore, the 12.2 arcmin aperture data was not used as a sole criterion for source detection. The background was estimated in a circular annulus surrounding each detection aperture with an area of 85 arcmin². For the smallest aperture, the annulus was the area between 3 and 6 arcmin in radius, and for each larger detection aperture the other background annuli were scaled up appropriately. The Poisson noise from both the source aperture and background annulus was also calculated. An initial scan of the data was made to find all possibly significant detections with a ratio of signal to Poisson noise exceeding 2.5 and a sufficient fraction of reliable pixels in the source and background apertures (roughly 60% and 30%, respectively). These fractions are less restrictive than the EMSS algorithms of necessity, since the larger detection apertures require that a larger fraction of potential sources are close to rib support structures and other,

brighter sources. Detection proceeded iteratively over the entire sky map, with the threshold count-rate decremented from an initial high value down to the 2.5 σ minimum. Pixels associated with detected sources at each iteration were masked out for successive iterations. The entire sky map was analyzed separately with each aperture.

A catalog of sources was then constructed from the three useful lists of detections, by matching them if the center of one detection fell within the aperture of another. A single source usually consists of multiple detections in each aperture. However, only one detection (with the highest S/N) was retained for each aperture and the others were discarded. A source was retained in the catalog only if there was a 4 σ detection in at least one aperture. The location of each source was defined to be the centroid computed as the weighted average of all the aperture centers \vec{x}_i ;

$$\vec{X}_c = \frac{\sum_i \vec{x}_i (R_i/\sigma_i)^{-2}}{\sum_i (R_i/\sigma_i)^{-2}}, \quad (1)$$

where R_i is the aperture size and σ_i the signal-to-noise in that aperture. This is only an approximation since it assumes that the measurements in the different apertures are independent, which they are not. The single-standard deviation uncertainty in the position is taken to be $\sim \min [R_i/\sigma_i]$, and we note that all source positions are accurate to better than one arcmin, with an average uncertainty of 28 arcsec.

A total of 7419 sources were identified in this manner. To eliminate contamination by Galactic emission or known sources of diffuse emission, only sources at Galactic latitude $|b| > 20^\circ$ were retained. Also, any sources within 5° of the Large Magellanic Cloud, 2.67° of the Small Magellanic Cloud, 2.67° of the Coma Cluster, or 1.6° of Messier 31 were excluded. At this stage, the IPC source list contained 6600 sources.

2.2. New Sources in EMSS Fields

The original EMSS catalog of 835 X-ray sources was compiled from serendipitous sources detected in 780 deg² within 1435 separate IPC images at $|b| > 20^\circ$ (Gioia et al. 1990b). To construct a list of new sources which can be directly compared with the EMSS, the 6600 IPC sources were culled to include only those sources which have measured count-rates above the required threshold for the corresponding field (i.e., sufficient to generate $\sigma > 4$ in the EMSS detect cell if the counts were concentrated in a point source profile), and those sources which fall within EMSS fields. These restrictions result in a catalog of 979 sources. It was also necessary to cull some of these 979 sources from the catalog because they would **not** have been included in the EMSS for other specific reasons described below.

To estimate the S/N that each source would have had in the EMSS detect cell, the source and background counts in the EMSS field must be predicted by including several factors:

To estimate count rates in the EMSS detect cell, the effective exposure time at the location of a source in each IPC image was calculated by adjusting the “live” time at the image center for large angle scattering by the X-ray telescope mirror (a factor of 0.847) and vignetting. The

⁵ A service of the Laboratory for High Energy Astrophysics (LHEA) at NASA/ GSFC and the High Energy Astrophysics Division of the Smithsonian Astrophysical Observatory (SAO)

vignetting function $V(\theta)$ derived by Harris et al. (1990) for 1.5 keV energies was adopted. As a function of the off-axis angle θ in arcmin it is given by

$$V(\theta) = 0.997 - 8.25 \times 10^{-3}\theta - 3.125 \times 10^{-4}\theta^2, \quad (2)$$

for $\theta < 12$ arcmin, and

$$V(\theta) = 1.1049 - 0.02136\theta, \quad (3)$$

at larger angles. At the 19 arcmin limit of each subfield, the vignetting correction is 0.70.

Second, the IPC background was assumed to be uniform in the vicinity of each source and the number of background counts was corrected by the ratio of the area of the EMSS detection aperture (5.76 arcmin²) to that of the aperture used in the actual detection. Additionally, the predicted total number of EMSS source counts calculated above was multiplied by the fraction of the point response function inside the EMSS detection cell (a factor of 0.885). A similar correction was *not* applied to the count-rates in the new apertures but that correction is quite small. Using the estimated EMSS detect cell source and background counts, we determined the significance of each detection. The S/N of each source was calculated using the formula

$$\sigma = \frac{C_S}{\sqrt{C_S + C_B}}, \quad (4)$$

where C_S is the source counts and C_B the background counts. The calculation was performed using the source and background counts for each of the three smallest apertures corrected as described above. This calculation determines whether the newly discovered source would still be greater than 4σ in the EMSS catalog if a different aperture size had been used in the EMSS detection algorithm. We excluded any sources from the catalog that did not meet this requirement.

We then scrutinized the catalog to eliminate any remaining sources which should not be included in the EMSS. Only sources falling within specific annuli centered on each of the EMSS field centers were considered. The outer annulus border is a circle 19 arcmin in radius which lies just inside the IPC detector ribs and includes the most sensitive detection area. Within this radius the vignetting correction is less than 30% and is nearly unaffected by the satellite roll angle. The inner border is 6 arcmin in radius and preferentially screens sources which were the targets of pointed observations rather than serendipitous detections. Although this region is different than that used to construct the EMSS (a square 45 arcmin on a side with the central 5 arcmin removed), the restrictions can be applied *post facto* to the EMSS catalog to generate a subset of the EMSS catalog which can be directly compared to the new source list. To remove any overlap with the EMSS catalog, all IPC sources within 6 arcmin of any EMSS source are removed and, to remove duplications, all catalogued sources within 6 arcmin of another source are also excluded. Fifty-four such targets were identified and removed.

While the 19 arcmin maximum radius from the IPC center was imposed to avoid shadowing by the detector “ribs”, the IPC center is actually offset with respect to these ribs and, moreover, some sequence number frames are actually combinations of sub-exposures taken at the same sky location but at different telescope roll angles. The result of

these multiple exposures for the current analysis is that the rib pattern rotates with respect to the field. The combination of these two effects means that some sources at a radius $r < 19$ arcmin away from the field center still have non-zero rib-edge codes (i.e., vignetting by the IPC rib structure or the edges of the detector area are quantified by a “rib-edge” code, Harris et al. 1990; we have used the same rib-edge code criteria to eliminate sources as that described in Gioia et al. 1990b) and so would not have been included in the EMSS source catalog. To remedy this situation we have scrutinized individually for rib-edge codes (a) all sources with $16 < r < 19$ arcmin and (b) all sources detected in sequence numbers made up of multiple sub-exposures taken at different roll angles. Thirty-eight sources were excluded because they would also have been excluded from the EMSS due to shadowing by the ribs.

In some cases, due to a poorly known target position, the desire to observe other nearby sources in the field-of-view of the IPC or simply some other circumstance (e.g., mispointing), the target of the IPC observation was not within the 6 arcmin central region. Also some targets are quite large in angular size (e.g., M101, NGC 253, etc.) and so occupy more than 6 arcmin within the IPC field. We have eliminated both the specific mispointed targets of IPC observations, as well as sources which are related to the target (i.e., within the optical extent of very extended targets). Forty-eight sources were identified as the mispointed target of the observation and eliminated; 12 additional sources were eliminated for being related to very extended targets.

In addition, some regions of the sky were observed more than once by the IPC detector. In some cases, the additional exposures were fields *not* included in the original EMSS. For these fields, the S/N of any detected, non-variable source will be increased over the value that would be measured by using only the EMSS exposure time. We have individually investigated every set of merged fields (overlapping with the central coordinates of the fields coincident to < 1 arcsec) in the catalog. We identified those sources whose S/N would be reduced to less than 4 in the first three apertures if only the EMSS exposure time was used. We eliminate 55 such sources.

Finally, there exist multiple IPC exposures in some fields which overlap but are not coincident, thereby increasing the exposure time for only the overlapping regions. If the overlapping observation was not included in the original EMSS, a detected source will have an increase in measured S/N similar to the merged field scenario described above. The IPC detector area is so large that the number of such occurrences in the catalog is prohibitively large to investigate individually. It is also difficult to estimate the true effective exposure time in such overlapping regions because of the large variation in vignetting across the IPC field. In §5.1 we make a statistical estimate of the effect of these occurrences on the catalog due to overlapping non-EMSS observations.

Excluding sources for all of the reasons cited above (except the statistical estimate for multiple exposures to be applied later) results in a catalog containing 772 sources. An electronic version of the 772 source catalog can be obtained from the first author⁶.

⁶ <http://casa.colorado.edu/~lewisad/research/nemsscatalog.html>

While the new IPC sources are 772 in number, there are only 478 (of 835 total) original EMSS sources falling within the same restricted survey area. Figure 1 compares the 0.3 – 3.5 keV count rates calculated in the 2.5 arcmin aperture to the original EMSS values for 334 of these 478 sources. We have compared only sources thought to be point-like on the basis of their optical identifications (i.e., EMSS sources identified as either stars, BLLacs, or AGN; any EMSS source which is even possibly a combination of two or more sources has also been eliminated from this plot, see also a similar plot in OHG97). The agreement is generally very good and, significantly, there are not a substantial number of sources with OHG97 count rates significantly *higher* than EMSS values. Thus new sources are not being included due to some systematic upwards bias in the re-estimated count rate.

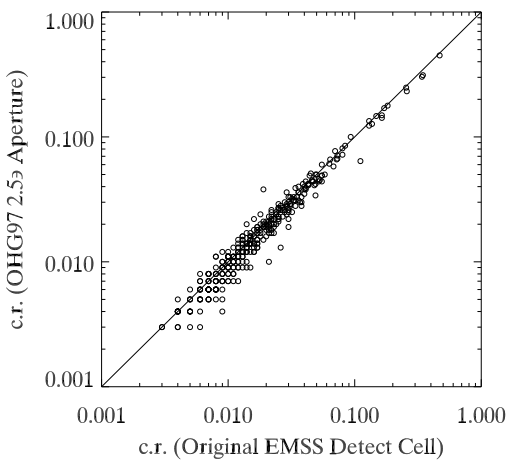


FIG. 1.— Comparison of the 0.3–3.5 keV count rates (c.r., in units of counts s^{-1}) estimated in the 2.5 arcmin aperture of the OHG97 catalog to those estimated by the EMSS (Gioia et al. 1990b) for 334 point-like EMSS sources within the central region of the EMSS fields. The solid line represents equivalence between the two estimates.

2.3. Estimates of Source Confusion

The use of apertures larger than optimal for point-source detection suggests the possibility that spurious detections may occur if more than one unrelated source with flux below the detection limit appears in the same aperture. The “excess” variance (over other noise sources) produced by point-to-point fluctuations in numbers of undetected sources in a beam has been traditionally exploited to constrain number counts below the detection threshold (e.g., Hamilton & Helfand 1987). Here, the hypothesis that such variations are responsible for a significant number of these new IPC sources is evaluated; i.e., the probability that more than one source is present in the detection aperture, which when combined obtains a count rate above the detection threshold.

A method that can be used to estimate the number of multiple sources in any one detection cell as a function of detected source flux is described in Stocke et al. (1991). Given the detection aperture area and a typical source flux for EMSS sources, S.L. & S.D. Morris (in Stocke et al. 1991) developed a probabilistic formalism which predicted that ~ 16 of the EMSS sources with $f_{0.3-3.5} \geq 2 \times 10^{-13}$

ergs $s^{-1} cm^{-2}$ were confused and were actually two sources of lower flux, which combine to make up the detected count rate. By “confused” it was meant that the second, fainter source contributed $\geq 20\%$ of the total flux in the detect cell (and thus contributed significantly to a 4σ source near the detection limit). The predicted number of confused sources (16 ± 4) was verified observationally in the EMSS by the number of X-ray source error circles which contained more than one plausible optical identification (ID); i.e., more than one plausible X-ray emitter based upon their optical properties was found for 10 sources at this flux limit and above. A few other cases have been found since that time based upon reobservation of EMSS sources using the higher spatial resolution of the *ROSAT* PSPC or HRI. Stocke et al. noted that, based upon their high surface densities, QSOs and stars are the most likely confusing source populations (i.e., pairs or multiples of point sources).

Using the scaling relations for source confusion with flux and aperture size given above, the EMSS baseline value for confusion can be extrapolated to the OHG97 methodology (the accuracy of which has been verified by the optical ID work of the EMSS team). Table 1 shows the results of these calculations, the percentages of preliminary catalog sources which are “confused”. Percentages are shown for the highest count rates encountered in the catalog, for the median count rate, for a low value of the count rate and for the lowest count rates encountered in the catalog as a function of the various detect cell aperture sizes used herein. Several conclusions can be drawn immediately: (1) as stated for other reasons before, the 12.2 aperture is not usable for making independent detections, being so large that virtually all but the brightest detections in that aperture are confused; (2) even the 8.4 aperture has a large fraction of confused sources at the fainter fluxes in the catalog and so sources detected only in that aperture must be viewed skeptically; (3) virtually all of the sources near the faint flux limit of the catalog are confused in all but the smallest aperture. Indeed, the values in Table 1 suggest that few sources below count rates of 0.01 are not confused. For reference, we show in Figure 2 the distribution of count rates for the entire 772 source catalog. We note that sources whose S/N was less than 2.5 in a particular aperture will not have a corresponding count rate value included in this histogram. Referencing Table 1, we can see from Figure 2 that there is a significant population of higher count rate sources which are not expected to be confused, particularly in apertures 2 and 3 at $> 0.02, 0.03$ counts s^{-1} , respectively.

TABLE 1

ESTIMATED PERCENTAGES OF “CONFUSED” SOURCES

Aperture Size (arcmin)	Count rate (cts s^{-1})			
	0.05	0.025	0.01	0.004
2.5	0.5%	1.8%	12%	50%
4.7	1.6%	6.6%	41%	100%
8.4	8.3%	21%	100%	100%
12.2	11%	45%	100%	100%

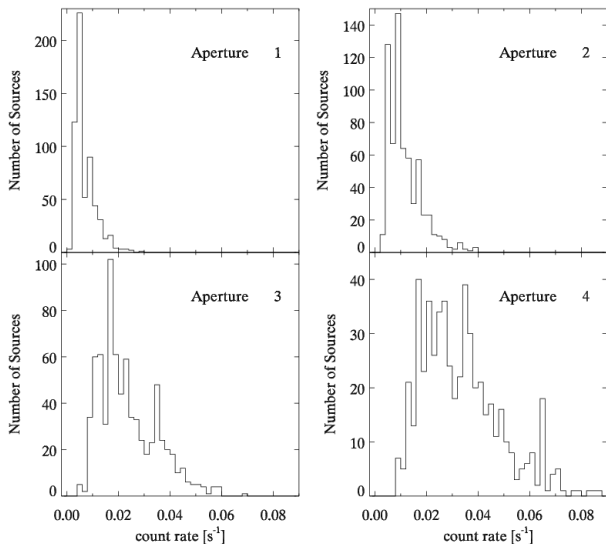


FIG. 2.— Distribution of the measured IPC count rates (in counts s^{-1}) for the 772 source catalog in each of the four apertures used in this work. Assuming a source spectrum of a 6 keV Raymond-Smith plasma with $n_H = 3 \times 10^{20} \text{ cm}^{-2}$, a source with count rate of 0.01 counts s^{-1} corresponds to an unabsorbed flux of $3.3 \times 10^{-13} \text{ ergs s}^{-1} \text{ cm}^{-2}$ in the 0.3 – 3.5 keV band.

3. INVESTIGATION OF A RANDOM SUBSAMPLE OF NEW IPC SOURCES

The putative new sources in a randomly-selected subsample of 133 of the 1435 EMSS IPC fields were examined in detail and compared with the original EMSS sources in those same fields. This provides an initial sample of practical size with which to scrutinize the reality of these sources and to determine their X-ray nature and identity. This sample size also facilitates a subsequent optical imaging study to determine whether clusters of galaxies are present among these sources.

3.1. Random Subsample Properties

The subsample fields were randomly selected without regard to sequence number, location on the sky, or exposure time, and thus can be considered representative of the entire collection of EMSS fields. The IPC sequence numbers of the observations are listed in Table 2. These fields include 73 new serendipitous sources and 49 original EMSS sources. Only 59 of the 133 fields contain even a single new source. Table 3 lists the basic X-ray properties for 74 sources⁷ including (by column): (1) the catalog number of the source; (2-3) RA and DEC in J2000 coordinates; (4) the IPC sequence number in which the source was detected; (5-7) the source count rates in the 2.5, 4.7, & 8.4 arcmin diameter apertures respectively (in units of $10^{-3} \text{ cts s}^{-1}$ in the 0.3 – 3.5 keV band); (8-10) the source statistical significances in these same three apertures in σ s; and (11) our final evaluation of the field, (C = definite cluster; C: = possible cluster; X = definite non-cluster; unmarked objects are unidentified due to a lack of information) based on information from the literature, X-ray databases, and our observing campaign, all described below.

⁷ Source # 4359, though included in Table 3, has been eliminated from the random sample, resulting in 73 random sample sources. See the footnote to Table 3, and discussion of the source in §3.2.

Based on the S/N values in the smallest aperture, very few of the new sources in the random subsample would be expected to be included in the construction of the original EMSS catalog. To check this we have measured the S/N of the sources in Table 3 in the 2.4 arcmin square detection aperture of the EMSS, based on the count rates in the 2.5 arcmin circular aperture used here (see §2.2). Because of the similar size of the two apertures these estimates should be very close to the actual values. (If the source was not detected within the 2.5 arcmin aperture, the signal within the smallest aperture with a detection was used). As expected, the vast majority (97% of detections in the smallest aperture) of sources have a S/N less than four in the EMSS detect cell and would not have been included in the EMSS. They are included here only because larger-sized apertures are used. A few sources would have had a S/N in the EMSS detect cell only marginally above four, yet they are not found in the original EMSS, suggesting that the exact size and shape of the detection **and** background apertures (when combined with small number statistics) can make small differences in the statistical significance of some sources.

Do the new sources found in the EMSS fields tend to appear more extended than the original EMSS sources? A larger apparent angular extent may be due to a single, extended source, a combination of two or more confused sources, or to a significantly softer X-ray spectrum, and would partially explain the failure to detect and include these sources in the original EMSS catalog. The X-ray surface-brightness distribution of a source can be qualitatively characterized by calculating the ratios of the count rates between the four different detection apertures used here. The apertures can be combined in three independent ratios: Here the fluxes in the three larger apertures were each divided by the flux in the next smaller aperture. These dimensionless ratios typically have values larger than unity as the larger aperture will tend to capture more flux than the smaller, but can occasionally be less than one due to Poisson noise or if there is a significant offset between the locations of the apertures. In Figure 3 the normalized distributions of flux-ratio for the 772 putative new catalog sources are compared to those of the 478 original EMSS sources within the the same inner regions of all 1435 IPC fields. These plots clearly demonstrate that the new sources tend to appear more extended than the original EMSS sources as measured by the ratios of the three smallest apertures. The Kolmogorov-Smirnov test of the null hypothesis that the two data sets are drawn from the same population yields probabilities of 1×10^{-39} , 1×10^{-46} , and 0.31 using the three respective ratios, $f_{4.7}/f_{2.5}$, $f_{8.4}/f_{4.7}$, and $f_{12.2}/f_{8.4}$. The large K-S probability for the third ratio is an additional reason for excluding detections made only in the largest aperture. Otherwise, the very small K-S probabilities for the first two ratios support the hypothesis that some of the new sources were not originally detected at a S/N > 4 due to an apparent lower X-ray surface-brightness, but it should be pointed out that there are substantial overlaps between the flux ratio distributions and this cannot explain all of the new sources.

TABLE 2
SEQUENCE NUMBERS OF A RANDOMLY-SELECTED SUBSET OF EMSS IPC FIELDS

207	305	421	443	444	454	470	478	481	498
500	505	797	852	863	889	1810	1937	2014	2030
2074	2082	2101	2127	2222	2602	2638	2716	2720	2911
3018	3070	3105	3176	3256	3263	3368	3453	3454	3471
3472	3530	3550	3816	3984	3988	3989	3993	4002	4037
4059	4147	4250	4261	4453	4499	4546	4577	4606	4621
4946	4972	5115	5125	5129	5191	5259	5388	5393	5397
5475	5504	5547	5652	5666	5670	5705	5708	5717	5796
5801	5929	6311	6317	6344	6407	6449	6646	6694	6728
6733	6746	6809	6835	6879	7036	7116	7165	7181	7204
7208	7426	7569	7582	7605	7636	7642	7668	7712	7719
7770	7771	7801	7803	7917	7957	7987	8047	8332	8334
8385	8433	8438	8439	8455	8458	8464	8740	8780	8838
8957	10382	10549							

We conclude that these new sources should not have been and were not included by the EMSS because they have too low a S/N in the EMSS detect cell, but are nevertheless detected with $S/N > 4$ using a different algorithm (i.e., the EMSS did not exclude these sources through some analysis mistake). The most likely causes for the rejection of these sources using the standard EMSS procedure is that they are either single extended sources, or collections of two or more point sources of lower individual flux. But, it is also possible that some point sources just below the 4σ detection limit in the EMSS rise to slightly above the detection limit in one of the new detect cells due to the difference in size and shape of the detection and background apertures, or the improvement in background determination.

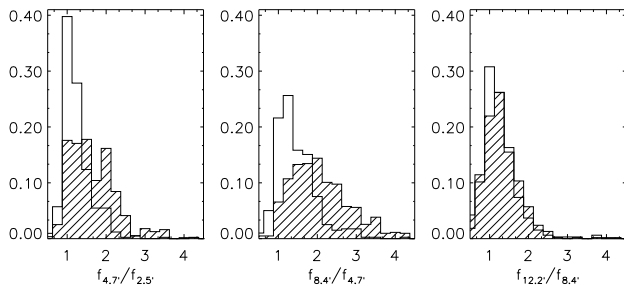


FIG. 3.— Normalized distribution of the ratio of fluxes in different IPC source-detection apertures for original EMSS sources (open histogram) and new (shaded histogram) source candidates in EMSS fields. Each histogram presents the ratio of successive pairs of apertures used to generate the catalog. Larger ratio values indicate that a source is more extended. In the first two histograms there is a clear statistical tendency for the new sources to have higher flux ratios than the original sources.

3.2. Database Search

Exhaustive searches of the NASA-IPAC Extragalactic Database (NED⁸) and the Stellar Information Database (SIMBAD⁹) were performed to search for plausible coun-

⁸ <http://nedwww.ipac.caltech.edu/>

⁹ <http://simbad.u-strasbg.fr/Simbad>

¹⁰ http://stdata.stsci.edu/dss/dss_form.html

¹¹ <http://legacy.gsfc.nasa.gov/cgi-bin/W3Browse>

terparts to each of the 73 new X-ray sources. Objects that are known sources of X-ray emission (i.e., clusters or groups of galaxies, AGN, nearby galaxies, and bright or double stars) within 5 arcmin of the X-ray position (and so potentially contributing to the X-ray flux in one or more of the three smallest apertures) were noted. Only 11 sources have plausible identifications; including 1 galaxy group at $z = 0.018$, 3 QSOs or AGN, 5 stars, and 2 IRAS galaxies, which are possible AGN. These sources are listed in Table 4, along with the references to these IDs, each of which has been checked for plausibility using the (f_x/f_V) method of Stocke et al. (1991). In Table 4 we also list one additional source (#4359), which was eliminated from the random subsample because it was related to the original target of the IPC observation (see §2.2). This source is clearly extended in a *ROSAT* PSPC image and there are many faint optical galaxies present on the Digitized Sky Survey¹⁰ (DSS) at its sky location. However, a few galaxies found in SIMBAD are at the same redshift as Abell 665, which was the target of the IPC observation in which source #4359 was discovered. Although this source is potentially scientifically interesting (a galaxy group falling into Abell 665?), the EMSS procedure would have eliminated this source and so we do as well.

The random subsample source list was next correlated with X-ray source catalogs generated from the RASS and other pointed observations made by *ROSAT* or *EXOSAT* using the facilities of the HEASARC¹¹ at NASA/Goddard Space Flight Center. Many detections were made in the vicinity (≤ 5 arcmin away) of random subsample sources, verifying them as bona fide X-ray sources. However, none of these sources were clearly resolved and only two sources (#4845 & #3564) had hardness ratios that are comparable to hardness ratios of previous X-ray cluster detections. Our optical imaging (described in §3.3) of source #4845 finds no cluster present so that the hardness ratio is not considered further here as a definitive discriminating characteristic. Table 5 presents the following information

concerning X-ray detections with $S/N > 4.0$ of the random sources made by other satellites (by column): (1) catalog number of the source; (2) the X-ray satellite and instrument which made the detection; (3) the percentage of the IPC flux that can be accounted for by the detected X-ray source(s) in the other instrument (in making this calculation we have assumed an energy index of $\alpha = 1.0$, which is appropriate for an AGN; i.e., a hard cluster spectrum would contribute a larger percentage, a soft stellar spectrum a smaller percentage than listed); the IPC flux used for the calculation is taken from the smallest aperture which includes the *ROSAT* or *EXOSAT* detection; (4) the angular offset between the random source centroid and the detected X-ray source (in arcmin); (5) the 3σ flux detection limit by the newer satellite image within 1.25 arcmin of the catalog source (i.e., in the sky region of the first aperture) if there was no *ROSAT* detection made within that region; (6) the database assessment of the angular extent of the detected X-ray source; (7) comments on the detected X-ray source(s); and (8) the evaluation of the random source identification based upon these X-ray detections alone.

These new observations can be used to eliminate conclusively some sources from being clusters of galaxies. Specifically, we eliminate all sources for which a reliable *ROSAT* detection (i.e., $S/N > 4.0$) is of sufficient flux to account for most or all of the IPC flux and is also time variable. Also PSPC detections accounting for most or all of the source flux which are found not to be extended sources are unlikely clusters of galaxies, and have been eliminated. This technique has been used successfully in several serendipitous *ROSAT* cluster surveys (e.g., Scharf et al. 1997; Rosati et al. 1998; Vikhlinin et al. 1998a). However, there are some PSPC sources which may be marginally extended and some that do not have determinations of extent available. These we have left unidentified. All of the HRI sources in Table 5 are listed in the *ROSAT* database as unresolved but, because the HRI is not extremely sensitive to extended flux, we do not use this information as definitive unless the HRI source accounts for the vast majority ($\geq 75\%$) of the IPC detection (i.e., there is little remaining flux that could be extended). Additionally, we eliminate those sources as potential clusters for which new *ROSAT* PSPC observations failed to detect a source within 3 arcmin of the catalogued source location to a limit significantly less than the IPC detection in the smallest aperture. Either these sources are variable and so are not clusters of galaxies, they are combinations of two or more sources flanking the new X-ray source location, or they are spurious in some way. By these criteria, we have identified 17 sources in Table 5 as not being clusters of galaxies (indicated with an X in column (8)).

3.3. Optical Imaging of Sources in the Random Subsample

To complete our study of the randomly selected sources, we conducted an optical imaging survey to determine if

any sources are in fact clusters of galaxies, the only plausible extended X-ray sources that could have gone previously undetected (bright nearby galaxies could be extended X-ray sources but are well catalogued and would have appeared in Table 4). Our objective was to obtain deep imaging of a sufficient fraction of the random subsample of new sources to make a statistical estimate of the number of X-ray clusters of galaxies in the catalog. Our target list for the imaging campaign was the 42 sources within the random subsample in the available RA range (0h-12h) and with declinations above -20 degrees. We note that our imaging program was designed to detect clusters out to $z \approx 0.8$. The optical imaging campaign is described in detail in Lewis, Ellingson, & Stocke (2001, Paper 2, hereafter).

The results of our imaging program are presented in Table 6, which lists by column: (1) the catalog number of the random subsample source; (2) comments for some fields; and (3) our evaluation of the field. In the majority of fields, the optical imaging alone, or in combination with the X-ray and other database searches, conclusively shows that no distant cluster is present. Three fields (#1757, #2036, and #4057) that were eliminated from being clusters based upon supplemental information unrelated to the imaging campaign (e.g., the existence of X-ray point sources found in the database investigations) are discussed in Appendix A. However, we did discover apparent galaxy over-densities in some fields, whose analysis we discuss briefly here (details of our method are given in Paper 2). Galaxies were detected, and colors and magnitudes were measured, with the galaxy photometry program PPP (Yee 1991). A color-magnitude diagram was constructed for each field, allowing an estimate of the redshift of any clusters or groups present, identified by a cluster-red-sequence (CRS, which is compared to the galaxy color models of Kodama & Arimoto 1997, and Kodama et al. 1998; our procedure is nearly identical to the method of Gladders & Yee 2000), as well as their over-density relative to the field, given by the B_{gc} statistic, (Yee & López-Cruz 1999). We present a discussion of the two sources we have identified as clusters or groups of galaxies here to elucidate our identification criteria. Optical images, color-magnitude diagrams, and detailed image analyses for these two sources are given in Paper 2. Unless otherwise stated, all fluxes are in the 0.3 – 3.5 keV energy band, unabsorbed, (corrected for absorption assuming galactic neutral hydrogen column density n_H given by $W3nH$ ¹²). Luminosities are K-corrected assuming a power-law spectrum with photon index $\Gamma = 1.5$ ($\alpha = 0.5$, following H92; consistent with a cluster spectrum in this bandpass) and quoted in the 0.3 – 3.5 keV energy band in the rest frame of the cluster.

Source #97: This source is identified as a nearby group of galaxies at $z = 0.018$ (NGC 181/183/184). We use the WPIMMS¹³ software to convert the third aperture count rate for this source to an unabsorbed X-ray flux of $f_X = 7.5 \times 10^{-13}$ ergs s^{-1} cm^{-2} in the 0.3 – 3.5 keV band. We also calculate an X-ray luminosity of $1.0 \times 10^{42} h_{50}^{-2}$ ergs

¹² Neutral hydrogen data is from Dickey & Lockman (1990). $W3nH$ is a Web version of the nH FTOOL. nH was developed by Lorella Angelini at the HEASARC. It is a service of the Laboratory for High Energy Astrophysics (LHEA) at NASA/GSFC and the High Energy Astrophysics Division of the Smithsonian Astrophysical Observatory (SAO).

¹³ $W3PIMMS$ is a Web version of the $PIMMS$ (v3.0) tool. $PIMMS$ was developed by Koji Mukai at the HEASARC. The first Web version was developed at the SAX Data Center. The SAX $PIMMS$ package was ported to and modified for the HEASARC Web site by Michael Arida. It is a service of LHEA.

s^{-1} in the 0.3 – 3.5 keV band, quite comparable to recent detections of similar, nearby, elliptical-dominated groups of galaxies (Mulchaey & Zabludoff 1998). The low redshift of this group makes the observed field of view too small to calculate a robust value for B_{gc} ; however, its optical appearance is quite similar to other poor groups of galaxies detected by *ROSAT* (Zabludoff & Mulchaey 1998). Additionally, the count rates for this source ramp to a significantly higher level in the larger apertures, as expected for a group subtending ~ 10 arcmin on the sky, rather than if this source were associated with just the largest elliptical in the group. A Green Bank catalog radio source appears associated with the dominant E galaxy as well. Therefore, we identify this source as a nearby group of galaxies.

Source #161: This source exhibits a high overdensity of galaxies across the field; however there appears to be more than one physical structure based on galaxy color and projected density. Accordingly, our over-density estimates have been corrected (to lower values) in an attempt to avoid contributions from galaxies at different redshifts. The galaxy over-density measurement is directly proportional to the number of galaxies detected in the field less the predicted field galaxy counts in that sky area, so we have segregated galaxies by color to assign them to each of the two concentrations, and corrected our over-density estimates by the fraction of galaxies in each structure (additional details can be found in Paper 2). We find that the most dominant sequence of galaxies lies within the redshift range $z = 0.52\text{--}0.59$. At a redshift of $z = 0.55$, we measure a galaxy over-density of $B_{gc} = 1340 \pm 560 (h_{50}^{-1} \text{ Mpc})^{1.77}$ (for a description of the uncertainty on the value of B_{gc} , see Yee & López-Cruz 1999). Combining the observed correlations of galaxy number density ($N_{0.5}$) with X-ray luminosity (L_X ; Edge & Stewart 1991) and B_{gc} value with galaxy number density ($B_{gc} = 33N_{0.5}$; Harvanek et al. 2001), we can make a rough estimate of the expected luminosity of such a galaxy over-density: $L_X(0.3\text{--}3.5) = 3 \times 10^{45}$ ergs s^{-1} , corresponding to a total X-ray flux $f_X = 2.3 \times 10^{-12}$ ergs $s^{-1} \text{ cm}^{-2}$. We convert the observed IPC count rates into fluxes to obtain $(1.4, 2.7, \& 5.1) \times 10^{-13}$ ergs $s^{-1} \text{ cm}^{-2}$ for the (2'5, 4'7, & 8'4) apertures, respectively. The estimated flux from this cluster is higher than the actual IPC aperture fluxes observed for this source so that this cluster is easily rich enough to produce the observed X-ray emission. The next richest concentration in the field lies in the redshift range $z = 0.32 - 0.38$. At a redshift of $z = 0.35$, we measure a galaxy over-density of $B_{gc} = 740 \pm 240 (h_{50}^{-1} \text{ Mpc})^{1.77}$. This corresponds to a luminosity of $L_X = 4.6 \times 10^{44}$ ergs s^{-1} , and a total $f_X = 8.9 \times 10^{-13}$ ergs $s^{-1} \text{ cm}^{-2}$ (i.e. 38% of the flux expected from the distant cluster). Thus, the more distant structure should dominate the expected X-ray flux. However, the apparent high redshift cluster is also 90 arcsec from our X-ray centroid, which suggests additional sources or extended emission could contribute to the X-ray detection. A marginal *ROSAT* HRI detection in a short exposure (7.8 ksecs) of this source is positionally consistent (17 arcsec N) with the two brightest cluster galaxies (BCGs) in the more distant concentration and has a flux consistent with being the sole contributor to source #161. Although not obviously extended, this source is detected at a S/N of < 3.0 and so is not a reliable indicator of

extent. In addition, there is an NVSS radio source consistent with one of the BCGs. Lastly, there is a galaxy approximately halfway between the position of the cluster and the X-ray centroid in Table 3. This object has $r - i$ color consistent with being a member of the $z = 0.55$ cluster, however its $g - r$ color is more than a full magnitude bluer. This suggests it is an AGN, but it is neither X-ray bright (not appearing as a source in the same exposure in which the BCG-centered source was detected) nor radio-loud (there is no NVSS source at its location though one of the BCGs was detected). Thus we can only assume that it does not contribute to the X-ray emission. The combined data therefore suggest that the more distant galaxy overdensity is of significantly higher flux than the nearer one, and is responsible for the IPC detection in this field. Due to the difference in position of the apparent cluster and the X-ray centroid, and the possibility of contamination by a second cluster or an AGN, we identify source #161 as a possible cluster of galaxies at $z = 0.52 - 0.59$.

In summary, the random sample of 73 sources contains one possible cluster of galaxies (#161, at $z = 0.52 - 0.59$) and one nearby group of galaxies (#97, at $z = 0.018$). The imaging survey, the database search and the cross-correlation with existing *ROSAT* data eliminates a total of 41 of the 73 sources from being clusters of galaxies. The remaining 30 have insufficient data at present to make an accurate assessment of the presence or absence of a cluster of galaxies. These 30 are in no way different from the rest, so that our sampling of this random subsample is itself random. Therefore, based upon our detailed evaluation of a random subsample of these new catalog sources we find one possible cluster (#161) and thus 0–1 out of 43 ($\leq 2.3\%$) sources are distant ($z \geq 0.14$, the limit for inclusion in the EMSS XLF evolution calculations) clusters of galaxies.

4. INVESTIGATION OF NON-RANDOM “SELECTED” SUBSAMPLES OF NEW SOURCES

The small number statistics in §3 are consistent with zero, or up to 18 ($2.3\% \times 772$ sources) additional distant clusters among the 772 sources in this catalog. The addition of 18 possible clusters would represent a significant change to the cluster XLF at high redshift. Therefore, it was necessary to hone our investigation to determine conclusively whether the catalog contains a significant number of new, distant clusters or not. To this end, we investigated two non-random subsamples, which were specifically chosen to maximize the selection of clusters and provide a robust lower limit to the total number of cluster to be added to the XLF. In this section we describe the investigation of sources within these two subsamples.

4.1. The “Ramp” Subsample

Assuming that a highly extended (or low surface brightness) source should increase its total flux (and therefore S/N given a uniform background) with increased aperture size, we selected a sample of sources wherein the S/N values increased (“ramped”) in larger apertures. Out of some 461 sources with appropriate RA and Dec. for our observing campaign, a total of 68 sources were found whose S/N in the four IPC apertures “ramped” appropriately. That so few new sources exhibit the S/N behavior expected for

extended sources is another indication that, as found in the random sample investigation, a typical catalog source is **not** a cluster of galaxies. But even this “ramping” behavior could mean either that flux from some point source offset from the catalog position was being detected in the larger aperture (although the two point sources would have to be separated by the correct amount on the sky to allow the S/N to increase systematically for all three apertures) or that more and more flux from a single, extended source was being included. It is also possible that other systematic effects could create changes in the S/N in any aperture, either masking or creating apparently extended sources.

Each of the 68 target “ramp” fields was investigated and given a ranking for observational priority. The investigation for each field included inspection of the DSS image for that field; a search for any known objects within 5 arcmin of the source location within the NED and SIMBAD databases; and an accounting of any known X-ray sources within the field from all public *ROSAT* and *Einstein* databases. Fields given first observational priority could have included some evidence of a galaxy over-density in their DSS image, and no evidence for multiple X-ray point sources in the field (which would indicate a combination of X-ray sources responsible for the new IPC detection). On this basis, 17 sources were assigned the highest priority, 6 of which were successfully observed. Lowest priority was assigned to fields with known QSOs or other non-cluster X-ray emitters present; none of these fields were observed. The remaining sources, lacking either of the above indicators, were placed as second priority; and 8 of these sources were also observed. The “ramp” sources observed are all typical of the first and second priorities, with individual fields chosen for observation simply on the basis of their sky availability during LST ranges not heavily populated with random sources listed in Table 3. The basic catalog X-ray data for the 14 sources observed optically (less than one quarter of the full “ramp” subsample), are listed in Table 7, with the same columns as Table 3. We note that there was no attempt in the creation of the “ramp” source list or in the observation of these sources to favor sources with high flux; i.e., the “ramp” sources are typical of catalog median values in their aperture count rates.

A summary of the database search and optical imaging results for the 14 observed fields are shown in Table 8 with the same columns as in Table 6. For each cluster candidate, the X-ray luminosity in the IPC bandpass of 0.3 – 3.5 keV was estimated from both the optical galaxy over-density B_{gc} , and the measured source count-rate in the IPC apertures (under the same assumptions used for source #161 described above). To be identified as a cluster of galaxies, the galaxy over-density was required to account for the majority of the observed X-ray flux. Four target fields (#992, #1310, #1492, and #1605) had apparent galaxy over-densities, and were the only “ramp” sources to be identified as clusters of galaxies. Images, color-magnitude diagrams, and details of the image analysis for individual fields are given in Paper 2. Note that source #992 was found to be target related, and was eliminated from the catalog (details are given in Appendix A).

With four distant clusters found in the examination of

only 14 “ramp” sources, or $\sim 30\%$ of candidates investigated, we find that this an extremely viable cluster selection technique.

4.2. The “High Flux/Signal-to-Noise” Subsample

Based upon the confusion statistics presented in § 2.3 and Table 1 as well as the random subsample investigation presented in § 3, a typical catalog source is likely to be either a combination of two or more lower flux sources and/or a single point source, whose presence in the new source catalog, but not in the EMSS, is due to the vagaries of small number statistics. With these two concerns in mind, we created a subsample of the catalog consisting of those sources with either the 50 highest X-ray fluxes, and/or the 50 highest S/N values. There was only modest overlap between the two criteria, resulting in a subsample of 92 sources. The highest S/N sources are the most likely sources not to be affected by small number statistics and so least likely to be single point sources not in the EMSS but present here (see § 5.1 for more details on this important point). The highest flux sources are those least affected by confusion (see Table 1). This source list comprises the best candidates for the purpose of discovering previously unknown rich clusters of galaxies in this catalog. We suggest that subsequent investigations of this catalog concentrate on these sources. We list in Table 9 the basic X-ray data for those sources which we observed from this sample. Columns are the same as in Table 7. We also note that two of the “Ramp” sources (#1492 and #1605) are also part of the high flux or signal-to-noise ratio (HFS) subsample, and that they were observed optically as a part of the “Ramp” subsample.

An optical imaging program for the HFS subsample, using similar priorities to those described in § 4.1 was undertaken in good weather conditions in May 2000. From a total of 20 observed fields, 11 contained apparent galaxy overdensities, and were further scrutinized to identify potential clusters. The results of the imaging program are shown in Table 10 (columns are identical to Tables 6 and 8). X-ray luminosities for cluster candidates were calculated in the same manner as for sources in the “ramp” subsample, and are given in Table 11, described below. Three sources are identified as clusters or groups of galaxies, and two additional sources are possible clusters due to some uncertainties within or inconsistencies among the observational data. The remaining six cluster candidates were rejected after detailed investigation, and are discussed in Appendix A. Images, color-magnitude diagrams, and details of the image analysis for individual fields identified as clusters are presented in Paper 2.

A database and literature search was conducted for all sources in the (HFS) subsample and some clusters were found that had been previously identified. These sources are discussed in Appendix A, and included in Table 11 below. In addition, 3 of the 11 apparent galaxy overdensities described above had a corresponding RASS Bright Source Catalog (BSC) or Faint Source Catalog (FSC) detection. These detections are listed in Table 10.

4.3. Identifications from Other X-ray Surveys

In addition to the systematic investigations of pre-selected subsamples, we have also checked our source list

versus on-going cluster identification programs by Perlman et al. (2000, The Wide Angle *ROSAT* Pointed Survey I (WARPS I)), Romer et al. (2000; the Serendipitous High-Redshift Archival *ROSAT* Cluster (SHARC) group¹⁴), and the 160 Square Degree *ROSAT* survey (160SDS, hereafter, Vikhlinin et al. 1998a,b). Each of these programs list clusters identified from serendipitously detected *ROSAT* PSPC sources. There were six sources found in both our catalog and that of another group (#420, #2203, #2616, #2626, #3175, and #3469), each is discussed in Appendix A. Sources #420, #2203, #2626, and #3469 are identified as clusters of galaxies, and we adopt their measured redshifts and luminosities (where available).

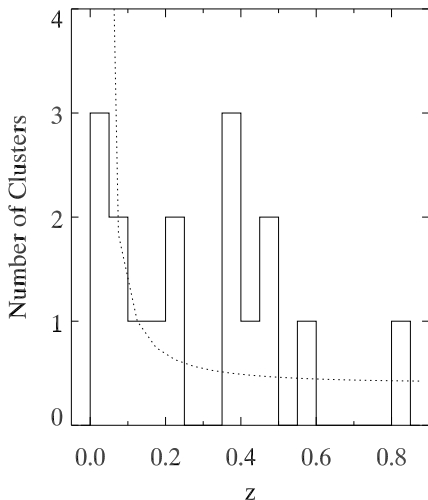


FIG. 4.— The redshift distribution of newly-discovered EMSS clusters; data from Table 11. The dashed line overlaid on the histogram indicates the expected number of missing clusters based on the ratio of EMSS detect cell flux to total flux (see §4.4), normalized to the number of objects in the bin containing $z = 0.14$. The distant, luminous clusters found in this work are in clear excess over that expected based on the H92 methodology in the redshift range ($0.3 \leq z \leq 0.6$).

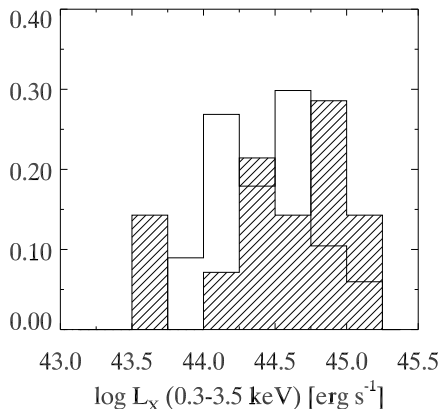


FIG. 5.— The normalized luminosity distribution of newly-discovered EMSS clusters (shaded histogram); data from Table 11. Overlaid is the normalized luminosity distribution of the original (H92) distant ($z \geq 0.14$) EMSS clusters (open histogram). The new clusters have very similar X-ray luminosities to the original EMSS clusters.

4.4. Summary of Non-Random Subsamples

In summary, our optical observations of pre-selected subsamples and investigation of available databases have found eight new or previously known clusters at $z \geq 0.14$, two $z \geq 0.14$ possible clusters, and five $z < 0.14$ clusters or groups (this accounting excludes Source #992, which was eliminated from the catalog, see Appendix A). Six of these sources are confirmed X-ray sources by *ROSAT* observations. A summary of data for these clusters (as well as those found in the random subsample) is shown in Table 11 which includes by column: (1) catalog source number; (2) spectroscopic redshift or estimated redshift range from photometry; (3) measured galaxy over-density, B_{gc} in $(h_{50}^{-1} \text{ Mpc})^{1.77}$; (4) log of the X-ray luminosity in $h_{50}^{-2} \text{ ergs s}^{-1}$ in the 0.3–3.5 keV bandpass calculated from the third IPC aperture flux; (5) log of the X-ray luminosity in ergs s^{-1} in the 0.3–3.5 keV bandpass either estimated from the B_{gc} value (see § 3.3), or as given by the reference for the source; (6) the subsample from which the cluster was identified; (7) notes on the nature of or identification for the cluster; and (8) the reference for the cluster discovery. We have used the data from the third IPC aperture to determine a total X-ray luminosity for these distant clusters. From the previously detected EMSS clusters at $z \gtrsim 0.2$ (Lewis & Stocke 2001), we find core radii of ≤ 50 arcsec so that $\gtrsim 90\%$ of the X-ray flux is contained easily within the third aperture assuming a standard β model. Even though some of these clusters may be more diffuse than previously detected EMSS clusters, the third aperture should contain the great majority of their flux.

For each cluster discovered in our optical imaging program, the detailed justification of the ID, estimated redshift, galaxy over-density, and X-ray luminosity is presented in Paper 2. Fields with apparent galaxy over-densities which nonetheless we identified as not being clusters are discussed in Appendix A. While this investigation is far from a complete accounting (i.e., only approximately 30% of the “ramp” and HFS subsample sources have been imaged, and the HFS subsample has an arbitrary lower limit), it is clear that this catalog does contain some previously undiscovered rich clusters. In Figure 4 we present the redshift distribution of the clusters in Table 11.

Based on the ratio of a cluster’s measured flux in the 2.4×2.4 arcmin EMSS detect cell (F_{det}) to its total extrapolated flux (F_{tot}), we can estimate the expectation for the EMSS to miss extended objects. The calculation of F_{tot}/F_{det} is shown in Figure 1 of H92 as a function of redshift. If we normalize this function to the number of clusters we have now discovered at redshift $z \approx 0.14$, it should indicate the relative amount of flux not measured, and therefore provide an estimate of the relative number of clusters which would be missed at other redshifts by the EMSS detect cell *if all clusters have surface brightness profiles described by a β -model with $\beta = 0.67$, and $r_{core} = 250 h_{50}^{-1} \text{ kpc}$, the canonical values assumed by H92. We have overlaid the curve of F_{tot}/F_{det} on Figure 4 (the dashed curve), showing the expected number of missing clusters, normalizing the curve to the histogram bin containing $z = 0.14$. Figure 4 shows the surprising result that the majority of new clusters are at a redshift*

¹⁴ <http://www.astro.nwu.edu/sharc/>

$z \gtrsim 0.35$, well beyond the $z \sim 0.1$ regime where one would expect to have missed clusters by using the formalism of H92. This result is unexpected only if clusters at all redshifts have similar structure (i.e., similar core radii and β values). The presence of so many new clusters at $z \geq 0.35$ may be due to the high- z clusters being more diffuse, and thereby missed in the EMSS due to a selection bias against low surface brightness sources. In detailed simulations, Adami et al. (2000) have shown that low surface brightness clusters (e.g., clusters with $\beta = 0.55$ or $r_{core} = 400h_{50}^{-1}$ kpc) have a significantly lower detection efficiency using the SHARC detection method, which is a wavelet-based algorithm specifically designed to detect extended objects. We expect that the EMSS method has an even more pronounced loss of efficiency for such clusters. Even if the new clusters are not extremely diffuse (e.g., Vikhlinin et al. 1998b, using an algorithm designed to detect extended objects, detected no significant increase in measured cluster core radius, assuming a standard β -model with $\beta = 2/3$ for clusters at redshifts $z > 0.4$ in the 160SDS compared with the nearby luminous sample of Jones & Forman 1999), it is plausible that the selection bias against extended sources was more severe than anticipated by the EMSS team. Due to the existence of high- z clusters near the flux limits of the IPC observations, the EMSS survey missed several clusters which we are now discovering. In Figure 5 we present the normalized luminosity distribution of the clusters in Table 11 (shaded histogram). We have also shown the normalized distribution in luminosity of distant ($z \geq 0.14$) EMSS clusters taken from H92 (open histogram). We can see from Figure 5 that the new clusters exhibit a similar range of luminosities as the original distant EMSS clusters.

5. IMPLICATIONS FOR THE EMSS CLUSTER SAMPLE

In this section we evaluate the results of this incomplete investigation of new X-ray sources in EMSS fields. We use the results above to make the most accurate determination of the actual number of new sources that could potentially be added to the EMSS. That is, based upon our detailed study of the random and non-random samples, some of the sources in the catalog would not have survived the detailed scrutiny to which EMSS sources were subjected (see Appendix A for individual examples). These must be eliminated, at least statistically, for comparison with the EMSS. We also use the number and estimated redshifts and luminosities of the new distant clusters we have found to infer the statistical impact on the EMSS XLF and its evolution.

5.1. A More Accurate Comparison Sample for the EMSS Source Catalog

Based upon the investigation of the catalog subsamples described in the previous sections, it appears that: (1) many of the catalog entries are the “confused” combinations of two or more fainter sources and thus not true additions to the EMSS; (2) many sources are single, likely point-like sources, which were not included in the EMSS for reasons as yet unclear (but perhaps due only to Poisson statistical fluctuations occurring between different size and shape apertures); (3) $\leq 2.3\%$ of the new catalog sources may possibly be distant clusters of galaxies, and we

have found several examples. A similar number of nearby ($z < 0.14$) poor clusters or groups of galaxies are likely to be present. If this is the case, and considering that the source catalog was generated from only a subset of the EMSS sky area, the impact on the EMSS X-ray luminosity function (XLF) could be significant. In order to estimate the impact on the EMSS cluster XLF as precisely as possible, in this section we scrutinize the catalog in more detail based upon our investigations in § 3 & 4. We will attempt to emulate the EMSS selection criteria as precisely as possible using knowledge gained from problems found in the random and non-random subsamples. This process will help us estimate the most accurate number of new sources to be added to the EMSS fields.

However, we emphasize that almost all of the corrections in this section are statistical in nature; i.e., it is not possible to determine which individual sources should be removed from the catalog (and which should stay) in order to make the most accurate comparison – we can only estimate the fraction of sources which should be removed. Therefore, the results of this section do not discredit the reliability of any individual source in the catalog; i.e., based upon the catalog evaluation presented in § 3, we believe that the large majority of these sources are real fluctuations above background, although most are superpositions of fainter sources.

We have edited the catalog (originally consisting of 772 sources) into a final EMSS comparison sample of 406 sources by the following four actions:

1. While we have shown in § 2.2 that the methods employed herein do not significantly bias the detected source counts relative to the EMSS, they have in fact modified the source detection method and background determination such that the S/N is higher for sources detected using the OHG97 algorithms when compared with EMSS values. Thus the catalog contains new sources within the EMSS sky area simply because faint X-ray sources in the same fields are now detected at $\geq 4\sigma$ while the EMSS detected them at $< 4\sigma$. This is the most likely reason why our imaging survey has concluded that some sources are single, point-like X-ray emitters. Since these sources appear in the new catalog only due to more favorable statistics, we conclude that these sources should not be added to the EMSS. Because it is impossible to identify exactly which sources these are, and in order to account for this bias relative to the EMSS, we artificially raise the detection limit for the larger apertures to correct for this effect statistically. To determine the new detection limit for the larger apertures, we show in Figure 6 the S/N of 334 EMSS sources thought to be point-like on the basis of their optical identifications (the same sample used for Figure 1, see §2.2). Figure 6 plots the original EMSS S/N versus the S/N of these same sources measured in the three smallest (2.5, 4.7 & 8.4 arcmin in diameter) IPC apertures. Since these EMSS sources are identified as single, unresolved X-ray sources, the differences found should only be due to the different detect cell sizes and detection methods employed herein. A similar plot, but for all redetected EMSS sources, can be found as Figure 5 in OHG97.

Figure 6 presents a good correlation between the signal-to-noise ratios determined by these different techniques, which reveals a mild systematic bias in favor of the

new background determinations and the circular apertures used herein (i.e., a systematically higher S/N compared to the original EMSS) but with a substantial scatter as well. Evidently, the Poisson statistical regime plus the slight differences in detect and background cell sizes, shapes, and locations and the different background maps combine so that some EMSS sources are redetected at higher S/N by the current technique and some are redetected at slightly lower S/N. The possibility of such variation in measured S/N was raised in § 3.1 where some random subsample sources were found to have a $S/N \geq 4$ in the original EMSS detection aperture, although of course they were not detected by the EMSS. This variation in measurement creates a dilemma for an accurate comparison between the present work and the EMSS since we cannot say absolutely whether any one source close to the 4.0σ detection limit should be included within the EMSS or not. Instead of attempting to scrutinize each source individually to estimate the EMSS S/N, we treat this bias statistically using the median ratios of S/N in the catalog relative to the original EMSS values, shown as dotted lines in Fig. 6. The new limits which correspond to 4.0σ in the EMSS are 4.1, 4.3 and 4.5σ for the 2.5, 4.7, and 8.4 arcmin apertures, respectively. We emphasize that these new detection limits still do not emulate the EMSS as closely as one would like because of the significant spread in S/N for the source detections, which are not related to the source being resolved with respect to the detect cell. Thus, “new sources” would be detected in the EMSS sky area even if all sources were point-like with respect to the detection aperture employed (and some “old” EMSS sources would not be re-detected for the same reason). Nevertheless, these new S/N limits statistically eliminate 261 ± 16 sources from the comparison sample (including two sources identified as clusters of galaxies, #1310 and #1492, and one low redshift galaxy group, #97).

We also note that even though the elimination of these low- σ sources provides a more accurate comparison with the EMSS, these sources are nevertheless likely to be real because the background determinations for them have been improved; they are just a bit too faint for secure inclusion in the EMSS.

2. As previously derived from theoretical considerations and verified in the imaging survey, many aperture 3 & 4 detections are likely to be confused. Some catalog sources were detected at $\geq 2.5\sigma$ in only apertures 3 and 4, which strongly suggests a combination of X-ray sources rather than a single extended source. We note that 9 such sources are present in the random subsample, four of which have *ROSAT* PSPC detections far enough away from the source position that the PSPC sources would not contribute any flux to the smallest aperture. A fifth source has a 9th magnitude star 4.6 distant, which is a very likely ID and again would not contribute any first aperture flux. None of the other 4 random sample sources in this category had either optical or X-ray database information. Our interpretation is that these catalogued sources are a confusion of a real (but $< 4\sigma$) offset source with other emission. What should have been a single source below the detection limit was buoyed up by circumstance, (e.g., proximity of rib structures or catalog boundaries to the background apertures, or nearby faint discreet sources) thus increas-

ing the S/N in larger apertures above 4σ . Had the offset source been $\geq 4\sigma$ by itself, the source centroid should have been closer to it. The automated detection and centering algorithms are so accurate that there are very few of this type of source. Therefore, we eliminate all such sources (53 in number) from the comparison sample.

3. The issue of overlapping (but not coincident, or merged) observations used to generate this catalog which were not included in the original EMSS was brought up in §2.2 but not addressed for the entire catalog. Though it is not feasible to investigate all such occurrences, we have instead conducted a detailed scrutiny of individual sources in the random subsample to identify how many sources suffer from such an overlap. We then estimate the decrease in S/N for each such source that would result from eliminating the non-EMSS observations. From the 73 sources in the random subsample, there were a total of 11 sources with overlapping fields. Nine sources were overlapped with rib-free regions of non-EMSS fields, and thus have potential extra flux from those exposures. There was no indication of variability in any of these 9 sources based on inspection of each sub-exposure. The remaining 2 sources had rib-edge code difficulties in one or more of the observations.

Of the nine sources with normal overlapping: six had exposure time corrections that would reduce the S/N in the first three apertures to < 4.0 , thereby eliminating them from the catalog; two had exposure time corrections that would not change their status – they remain in the catalog; the two remaining sources were overlapped by a rib-region of the IPC field, resulting in vignetting. One of these sources would remain a catalog source, assuming a maximum correction to the S/N based on the total exposure time. The other would be removed ($< 4.0\sigma$) under the same assumptions, although the actual vignetting is not known and would lessen the affect of this estimate. Any undetected source variability could affect the estimates significantly by increasing or decreasing the amount of flux detected during valid EMSS observations relative to the total flux. Thus we estimate that $10 \pm 1.4\%$ (7 ± 1 of 73) of the random subsample catalog are present due to the addition of non-EMSS overlapping exposures, and should therefore be eliminated from the comparison sample.

Because it was not possible to scrutinize the entire source catalog at the same level of attention as the random subsample, we have assumed that a similar percentage of sources in the final catalog suffer from the overlap scenario (i.e., $10 \pm 1.4\%$). Therefore, although we cannot identify which individual sources these are, we reduce the number of catalog sources for statistical purposes by 10% to account for these additional problems.

4. There was one source listed in Table 3 (#4359) which, after significant optical followup and database scrutiny, was eliminated as being target related. In this case, the source appears to be a portion of the X-ray emission from Abell 665, the target of the original IPC observation (see Appendix A). Another two such sources were found in the detailed investigation of non-random sources, and so this effect could occur in modest numbers in the full catalog. A few similar sources were removed from the EMSS after some optical and database followup work and could not have been found prior to such detailed investigation.

Since all catalog sources have not been scrutinized in this way, only a statistical culling is possible. On the basis of the random subsample evaluation, we eliminate 1.4% (1 of 73) of sources as being target related in this pernicious manner.

After culling the catalog using these new criteria, the number of sources in the final comparison sample is 406 ± 17 . The error estimate on this number is an in-quadrature combination of the various error estimates for the individual statistical subtractions made above. This number is comparable to the 478 EMSS sources found in the same sky area. We emphasize that this number is statistical in nature and (except for point #2 above) we cannot with high confidence identify individual sources which should be eliminated from the catalog. Therefore, we retain the full source catalog and will make it available electronically upon request to the first author.

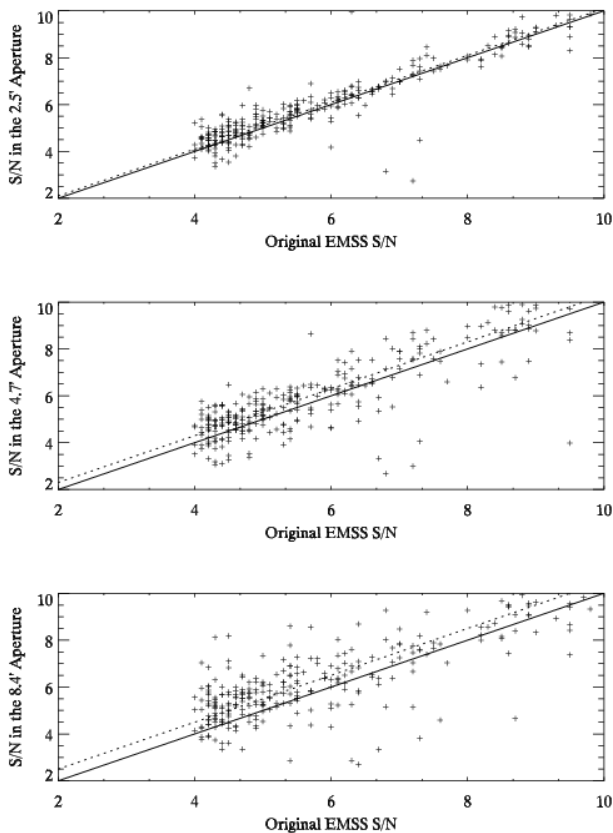


FIG. 6.— S/N of 334 point-like EMSS sources tabulated in the EMSS catalog vs. S/N measured in the 3 smallest apertures used in this work. The solid line is the one-to-one ratio expected if there were no bias between apertures. The median bias found in each aperture is shown by a dotted line; relative to the EMSS detection limit of 4.0σ , the bias corresponds to values of 4.1, 4.3, and 4.5σ for the 2.5, 4.7, and 8.4 arcmin apertures, respectively. However, note the significant spread in ratio values for all apertures.

5.2. The Effects on the EMSS X-ray Luminosity Function (XLF)

Applying the $\leq 2.3\%$ estimate of distant clusters found among the random sampling of new sources in §3.3 to the final number of EMSS comparison sources (406) arrived at in §5.1 suggests that there are a total of ≤ 9.4 “new” clusters in the comparison sample for the EMSS

(and ≤ 18.0 clusters in the entire 772 entry catalog). A comparable number of low-redshift ($z < 0.14$) poor clusters and groups are also expected based upon our random sampling. Our investigations have already found 11 new distant clusters and 6 nearby clusters or groups in the entire catalog. Counting the three possible clusters as only a one-half detection, and removing objects which would not pass the S/N cut made in § 5.1 (#97, #1310, & #1492), reduces these numbers to 7.5 and 5, respectively. All of our distant cluster detections above the S/N cut are in the HFS subsample excepting the possible cluster #161.

Thus we may set a value of 7.5 new distant clusters as the firm minimum addition to the EMSS sample. However, we have only partly investigated our catalog. Assuming that new cluster detections will only come from the HFS subsample (which is conservative; source #161 may be a distant cluster, and is not part of the HFS subsample), we can estimate how many clusters are in the full HFS subsample based upon how much of that sample we have yet to observe. Our optical observations to date have allowed evaluations of 26 fields in the HFS subsample (although Table 10 has only 20 entries, 6 sources observed as part of our investigations of the “Ramp” and Random subsamples are also HFS sources). In addition our database and literature investigations have resulted in 15 further identifications. Thus 51 of 92 HFS sources remain unidentified and unobserved optically. Assuming the same distribution of identifications as the observed sample, we estimate that within the remainder of the HFS subsample 5.6 distant clusters, 1.9 nearby clusters or groups, 3.7 possible clusters, and 31.8 non-clusters are present. Reducing these numbers by $10 \pm 1.4\%$ to account for sources in overlapping fields (see § 5.1) results in 5 distant clusters, 1.7 nearby clusters or groups, 3.3 possible clusters, and 28.6 non-clusters. Counting possible clusters with half weight, we arrive at a range of 7.5 – 14.2 new clusters in the entire catalog. This number is clearly conservative, assuming as it does that all new clusters will only be found in the HFS subsample, with no clusters below the arbitrary flux/count rate limit of that sample. Since the EMSS detected 37 distant and 12 nearby clusters in the same sky area as surveyed by this reanalysis, the EMSS distant cluster sample as presented in H92 is estimated to be 72–83% complete.

The nearby poor clusters or groups of galaxies we have discovered were missed by the original EMSS because they are so large on the sky that most of their flux falls outside of the EMSS detect cell. This eventuality was foreseen by Gioia et al. (1990a) and H92 who excluded the redshift range $z \leq 0.14$ from the EMSS XLF determination because of the very large correction that was needed to correct the EMSS detect cell flux to a total flux. In addition, the original EMSS catalog did not expect to be complete at $z \leq 0.14$ due to the fact that clusters of galaxies at these redshifts were frequently the targets of the IPC observations and therefore excluded from the serendipitous EMSS catalog. Thus the new $z \leq 0.14$ clusters found in the catalog will not impact the EMSS XLF determination at all. However, the addition of new, distant clusters to the EMSS could modify the XLF significantly, particularly in the high- z , high- L_X bins, where the current EMSS cluster numbers are quite small.

In order to construct a revised cluster XLF, we must first update the EMSS XLF, based upon work more recent than H92. The H92 XLF sample of clusters contained 67 clusters at $z > 0.14$, and $L_X > 5 \times 10^{43} h_{50}^{-2}$ ergs s^{-1} . The sample was binned for the calculation of the luminosity function at different redshifts. Three redshift bins at $(0.14 < z < 0.20)$, $(0.20 < z < 0.30)$, and $(0.30 < z < 0.60)$ were each subdivided into 6 luminosity bins, $(0.5 - 1.0)$, $(1.0 - 2.0)$, $(2.0 - 3.98)$, $(3.98 - 7.94)$, $(7.94 - 15.85)$, and $(15.85 - 31.62) \times 10^{44}$ ergs s^{-1} . Since then, subsequent work has modified these original cluster data somewhat; details of the changes and updates can be found in Lewis (2001). These changes include new or revised cluster redshifts and/or luminosities measured since H92, as well as revised identifications primarily based upon a systematic *ROSAT* HRI imaging program of possible BL Lac objects originally identified as clusters of galaxies (Rector et al. 1999). One source, MS 1317.0-2111, was not detected in the *ROSAT* HRI campaign for unknown reasons, and so we leave its ID = cluster as in H92. In Figure 7 we show the EMSS XLF in three redshift shells. Open circles are the original EMSS data taken directly from Figures 2 and 3 in H92, open triangles reflect all of the corrections we have just described. We have recalculated the luminosity function using the updated data, following in every detail the prescription for calculating search volumes as described in Gioia et al. (1990a), H92, and Henry (2000) in order to match the H92 results. However, there are now clusters in the EMSS sample at $z > 0.60$, and so a fourth redshift shell ($0.60 < z < 0.85$) has been added to accommodate all clusters now in the sample. We will truncate the volumes for clusters in the third shell ($0.30 < z < 0.60$) in exactly the same manner as H92. The resulting XLFs are shown in Figure 7. None of the values change beyond the 1σ errors, but note that the largest changes are in the lowest luminosity bins.

After making these corrections, we now use the newly discovered clusters in this catalog to estimate the full number of new EMSS clusters that should be added to each (z, L_X) bin in the full EMSS sky area. The estimated redshift range of each distant cluster in Table 11 place it in a single redshift bin; however, our luminosity estimates in a few cases span more than one luminosity bin. We have therefore added ‘fractional’ clusters to the appropriate luminosity bins. Furthermore, three of the clusters in Table 11 (#161, #2844, and #2906) are only possible cluster identifications. Conservatively assuming a 50% false identification rate for possible clusters, we add one-half cluster to the relevant (z, L_X) bins for each of these sources.

Based on the results from § 5, there are ≤ 9.4 distant clusters in the comparison sample of 406 ± 17 objects. Based on the actual number of detected clusters in the catalog, and the estimate of clusters not yet found within the HFS subsample given above, there are 7.5–14.2 distant clusters in the catalog. As the two estimates are consistent, we will adopt the latter as it is based on a larger number of actual detections. However, both estimates are drawn from the limited sky area of this work. The original EMSS sky area included the full unobstructed field of view of the IPC detector, whereas we have used only the inner 19 arcmin of each field. A direct scaling of the sky areas used would be inappropriate because the outer regions

of the detector have lower effective exposure times, along with other effects. However, an approximation to the correct scaling is the number of EMSS sources detected in these two different sky regions. A total of 478 of the 835 total EMSS sources fall within the restricted survey area of this catalog. Using this scaling increases the number of missing clusters expected in the full EMSS sky area to 13.1 – 24.9.

Making the assumptions that the redshift and luminosity distributions of currently undiscovered clusters in the EMSS sky area match those we have currently discovered, we add clusters to the redshift and luminosity bins accordingly. In Table 12 we show the original EMSS XLF data of H92 modified to reflect the updates from more recent work described above (first entry in each bin). Additionally, we show the number of clusters in each bin resulting from the additions of only those clusters we have found thus far in the catalog (Table 11; second entry in each bin). The third entries, shown as a range, are our best estimate of the total number of clusters we expect to exist in the EMSS, by adding the estimated total new cluster numbers. Note that we have added a fourth redshift shell, $0.60 < z < 0.85$, as described above; we do not combine it with the $0.30 < z < 0.60$ shell in order to better compare with the H92 results.

In order to calculate the new XLF including the addition of new clusters, we must calculate the accessible volume (V_a) for each additional cluster to find its contribution to each (z, L_X) bin. Based in part on the method detailed in H92, we calculate the luminosity function (taking care to appropriately weight possible clusters whose estimated L_X spans more than one bin). The volume V_a for each cluster must be calculated based on its detect cell flux, F_{det} . Because our new clusters were not detected using the EMSS detect cell, we must estimate the value of F_{det} that the EMSS would have obtained. Earlier (see §4.4) we argued that the 3rd (8.4') aperture is a good estimate of the total X-ray flux from these distant clusters (see Lewis 2001, for details). We then assume the same conversions between F_{det} and F_{tot} as used by H92 and Gioia et al. (1990a) to calculate V_a for each new cluster according to the prescription of Gioia et al. (1990a), H92, and Henry (2000), and so obtain $N(L)$ in each bin. We note that we take into account the IPC PSF, and the finite extent of a cluster’s emission (as described in Henry 2000) in performing our corrections. This procedure slightly overestimates V_a (due to a slight overestimate of the detect cell flux for diffuse clusters; Adami et al. 2000); new X-ray images of these clusters would be required to obtain more accurate F_{det} and F_{tot} values. We emphasize that assuming canonical surface brightness profiles for the new clusters ($\beta = 2/3$; $r_{core} = 250 h_{50}^{-1}$ kpc), even though our detection algorithm implies they are more diffuse, conservatively reduces their impact on the XLF described below. With accurate surface brightness profile data in hand, we would expect to calculate lower V_a values, and thus greater $N(L)$ values in each bin.

The “negative” evolution of the XLF reported by H92 was based on the difference in the XLF between the lowest and highest redshift shells (see Fig. 3, H92) primarily in the fourth luminosity bin ($44.6 \leq \log L_X \leq 44.9$ ergs s^{-1}) where the XLF data differed at the 3σ level. In Figure 8

we show the EMSS XLFs in the first ($0.14 < z < 0.20$; filled circles) and third ($0.30 < z < 0.60$, open circles) redshift shells. These data include all the updates to the EMSS sample since H92 as well as the full addition of new clusters that we estimate to exist in the entire EMSS sky area from the current work (third entries in each bin, Table 12).

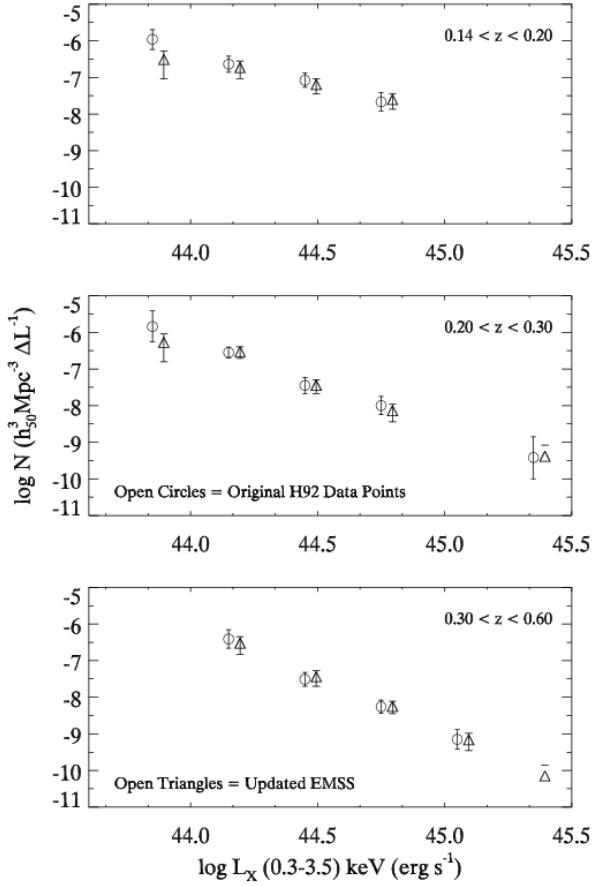


FIG. 7.— The X-ray Luminosity Function for clusters of galaxies in the EMSS sample in three redshift shells. Open circles are the original EMSS values as given by H92 (taken directly from Figures 2 and 3 in that work), open triangles indicate the values after updating for more recent work since H92 (the open triangles have been offset by $0.045 \log L$ for clarity). Error bars are 1σ errors computed from the number of objects in that bin using Poisson statistics. These values do not include the addition of any new clusters found in this work.

The addition of only a few clusters at high redshift and luminosity, both due to new data on existing EMSS clusters and to the estimated number of new clusters from this work, just barely allows the error bars in all the mutual L_X bins to overlap at the 1σ level. So we have reduced the strongest evidence of evolution (in the fourth L_X bin) to only 1σ . In order to make a better estimate of evolution in the XLF, we have overlaid the XLF derived from the $z \leq 0.3$ Bright Cluster Sample (BCS) of Ebeling et al. (1997) as a dotted line in both panels of Figure 8. We can see that in the right panel (new data) the fourth luminosity bin ($44.6 \leq \log L_X \leq 44.9 \text{ ergs s}^{-1}$) is now entirely consistent with the BCS XLF. The fifth and sixth bins do show a small deficit of clusters relative to the BCS. Taking into account the error bars from the BCS, the two samples differ only at the 1σ level in any individual bin. Thus, we

do not require evolution in the XLF at any X-ray luminosity. The deficit of clusters between our estimated high- z EMSS XLF and the BCS XLF is only 5 and 2 clusters in the fifth and sixth L_X bins, respectively. Given that our estimates of new clusters in the EMSS are conservative in basing total additions solely on the HFS subsample, seven additional clusters in the full catalog would not be surprising. These results differ from the recently renewed measurements of high- L_X evolution found by some other groups (see Gioia et al. 2001, for a thorough summary).

6. DISCUSSION AND CONCLUSIONS

In summary, a re-analysis of the complete *Einstein* IPC image data with improved detector-response information and a multi-aperture detection algorithm has generated a catalog of 6610 X-ray sources. Of these, 772 sources are detected within a subset of the EMSS sky area. The vast majority of these potential new sources (97% of the random subsample) would have had insufficient flux in an EMSS-like detection aperture to merit inclusion in the original catalog and were detected here by using larger apertures. A statistical analysis of the relative fluxes in the four apertures used in the source detection algorithm indicates that these new sources appear more spatially extended than the original EMSS sources. There are several possible explanations for why these sources were not included in the original EMSS: (1) improved flat fielding has reduced systematic errors in the detection process, resulting in the recovery of additional EMSS-like sources; (2) these sources tend to have softer X-ray spectra (e.g., those of stars) which emit primarily at lower energies where the width of the X-ray telescope-IPC point response function is larger and makes these sources appear more extended and thus less likely to have been detected in the EMSS; (3) some of these sources are related to targets, are affected by the telescope ribs, or have S/N values that are increased by contributions from non-EMSS exposures; (4) many of these sources are actually physical or projected aggregates of sources which individually are below the flux limits of the EMSS but have the necessary ensemble flux at angular scales corresponding to the large apertures used here; and (5) these sources are actually spatially extended objects. Only explanation (2) can be eliminated from being the reason for many of these new sources. The spectral characteristics of the *ROSAT* PSPC counterparts to some of these sources do not support the hypothesis that the majority of these sources are spectrally soft, nor have we identified many of these sources as being due to stars. All of the other explanations appear to contribute substantially to the catalog.

Primarily to distinguish between explanations (4) and (5), we scrutinized a random subsample of new sources. In a randomly-selected subset of 133 IPC fields there are 73 new serendipitous source candidates (compared with 49 original EMSS sources within the same area of sky), which have been investigated through database searches and optical imaging, revealing that the vast majority of sources are not clusters of galaxies. One possible new distant cluster ($z = 0.52 - 0.59$) and one nearby group ($z = 0.018$) were found. The possible distant cluster detection in this sample implies that $\leq 2.3\%$ (0–1 of 43 random sources) of the catalog are distant clusters.

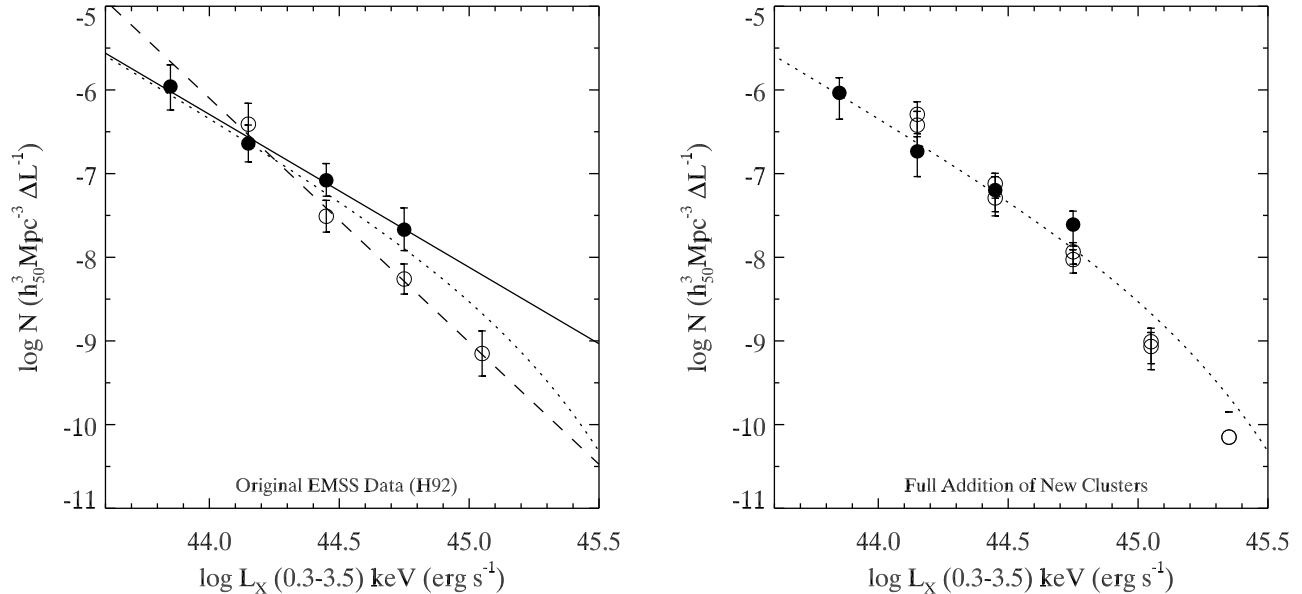


FIG. 8.— The X-ray Luminosity Function for clusters of galaxies in the EMSS sample in the first ($0.14 < z < 0.20$; filled circles) and third ($0.30 < z < 0.60$; open circles) redshift shells. The left panel shows the original XLF determinations of H92. The right panel shows our revised values based upon the addition of new clusters from the HFS sample after scaling for the number expected to be in the full EMSS sky area (there are two open circles in each bin, the lower range is the sky area scaling of only those 7.5 clusters already found in the HFS sample, the upper end of the range includes the extrapolation of clusters we would expect to find if we investigated the remainder of the HFS sample, also sky area scaled; see Table 12, and § 5.2). The corrections and updates shown in Figure 7 are included here (in the right panel) as well. The solid and dashed lines in the left panel are power-law fits to the low and high- z redshift shells, respectively. Errors on the data points are the square-root of the total number of objects in each bin. The XLF from the BCS sample (Ebeling et al. 1997) is overlaid as a dotted line.

Specifically targeting different subsets of the catalog, which we pre-selected to be more likely clusters of galaxies, we searched available databases, the literature, and *ROSAT* surveys from other groups for cluster identifications. In addition, we conducted an imaging survey of 34 pre-selected sources. This investigation yielded 11 distant ($z > 0.14$) clusters (3 of which are only possible cluster identifications). Over half of these clusters are confirmed as X-ray sources by available *ROSAT* PSPC and HRI images. These clusters are missing from the EMSS, and many of them have large estimated galaxy overdensities consistent with high X-ray luminosities. Having confirmed the existence of a modest number of rich, distant clusters in the catalog, we further scrutinized the catalog to create a comparison sample as accurately matched as possible to the EMSS selection criteria. This allowed us to estimate statistically the EMSS catalog incompleteness. Using only the newly discovered clusters as a minimum, and our discoveries scaled to the full EMSS sky area catalog as a maximum, we estimate the EMSS cluster catalog of H92 to be 72 – 83% complete. These new clusters are plausibly lower in X-ray surface brightness than previous EMSS detections and could be clusters still in the process of virializing. As such, the examples found here may contain somewhat different galaxy populations than those found in X-ray luminous clusters heretofore (e.g., Ellingson et al. 2001). Source #420, for example, is clearly asymmetric and spatially extended, though it lies at very high redshift, according to the detailed analysis of its *ROSAT* PSPC image by (Ebeling et al. 2000, see also Appendix A).

Furthermore, the measured X-ray temperature of source #420 is $6.46_{-1.19}^{+1.74}$ keV (Della Ceca et al. 2000), approximately half the value found for MS 1054.4 – 0321 (Donahue et al. 1998), a cluster with nearly identical redshift and X-ray luminosity, suggesting that these two clusters are in very different dynamical states. Therefore, as shown in Della Ceca et al., the $L_X - T_X$ relationship must have considerable spread at $z \sim 0.8$, as would be expected if the evolutionary status of clusters at that epoch is much more diverse than today. In addition, the specific sources #1492, #1605, and #2436 are our best examples of such clusters since these clusters appear significantly richer in galaxies than their X-ray luminosity would indicate (see Table 11). Additional details of the optical imaging program and the optical properties of these new clusters can be found in Paper 2.

We then estimated the effect that these missing clusters would have on the EMSS XLF and its evolution. First, we have made corrections to the original EMSS cluster identifications, redshifts, and other particulars based upon new information available since H92. Then we add the newly discovered clusters to the sample, recalculating the XLF in the same redshift shells used by H92. While there are changes to nearly all the redshift and luminosity bins, the majority of cluster additions occur in the intermediate and high- z , high- L_X bins. Our additions have reduced the deficit of high redshift clusters in the fourth luminosity bin to 1σ , nearly removing the strongest evidence for evolution in the EMSS cluster XLF. Comparing to the BCS cluster sample, we do not require evolution in the XLF within any

luminosity bin for consistency at high and low redshift at the 1σ level. Our expectation for the number density of clusters in the EMSS at $0.3 \leq z \leq 0.6$ is lower than the BCS values at $z \leq 0.3$ in the fifth and sixth luminosity bins, equivalent to a deficit of only 5 and 2 clusters respectively. Because our estimates for the number of clusters missing from the EMSS were conservative, it is plausible the high- z EMSS XLF is entirely consistent with the BCS XLF. We caution, however, that the full number of new clusters in this sample is not known to great precision, and further optical imaging of these sources is required to be certain. The cosmological constraints from our result are complex, and without accurate X-ray temperatures, or other mass estimators for the new clusters, we cannot be definitive. However, most cosmological models constrain luminosity evolution in clusters and the basic trend is that for small values of Ω_{matter} , clusters evolve slowly, and for high values they evolve more rapidly (see e.g., Edge et al. 1990). Our addition of clusters mildly decreases the existing evolutionary constraint, which when combined with mass estimators, sets an upper limit to Ω_{matter} , slightly decreasing the allowed values from the limits set by Donahue & Voit (1999) of $\Omega_{\text{matter}} < 0.45 \pm 0.1$ for an open Universe, and $\Omega_{\text{matter}} < 0.29 \pm 0.1$ for a flat Universe. Future X-ray temperature measurements with XMM-*Newton* as well as optical velocity distribution data for these clusters will solidify these new constraints.

While the EMSS cluster sample suffers significantly from the use of a single, fixed detect cell size, it also has substantial advantages over other, more recent samples, which warrant its continued investigation: (1) the EMSS source selection is not based upon the X-ray source being resolved as with newer surveys (e.g., WARPS, SHARC, Rosati et al. 1998) such that highly concentrated X-ray clusters (if they exist) would not be misidentified (see Donahue et al. 2001); (2) virtually all EMSS sources have been optically identified (we do note that the large sky-area NEP sample is also virtually completely identified; Gioia et al. 2001), and indeed, even further scrutinized (e.g., the work of Rector et al. 1999, has found several sources originally identified as low (L_X, z) clusters that are actually BL Lac objects) making the optical identifications more secure; and (3) many IPC-detected clusters were reobserved, either as pointed targets or “serendipitously”, allowing a more detailed surface brightness analysis than is possible for new *ROSAT* detections. This latter advantage allows a much more secure correction from observed flux to total flux than for other samples and will be used to provide a final EMSS XLF determination in the third paper in this series (Lewis & Stocke 2001).

Finally, we emphasize that, despite the uncertainties in this analysis due to the incomplete optical identification of the full 772 source catalog, enough bona fide new distant clusters were discovered to cast doubt on the evidence

for evolution in the cluster XLF out to $z \sim 0.5$. Further, the reason for this new conclusion is the recognition that the original EMSS cluster sample is surface brightness, not flux-limited, and missed several high- z , high- L_X clusters due to this selection bias. And while the EMSS detection methodology may be the most susceptible to this bias, other cluster detection techniques (e.g., wavelet, VTP) probably have this bias present to a lesser degree (see Adami et al. 2000). Therefore, it cannot be assumed that *any* current X-ray discovery technique has detected all low surface brightness clusters above their stated flux limit.

The authors wish to thank all those who shared data and information with us, including Tadayuki Kodama, Isabella Gioia, Eric Perlman, and Kathy Romer, and especially an anonymous referee who pointed out a significant error in our assumed maximum redshifts, leading to an important correction to our results. ADL wishes to thank the KPNO support staff during the observing runs for this project, Michael Harvanek for help with data analysis and reduction, the HEASARC facilities for maintaining invaluable research tools and databases, and Beth White for her ongoing support. ADL made extensive use of the relations summarized in Hogg (1999), and gratefully acknowledges that author. ADL and this work were supported by a NASA Astrophysical Data Program grant #NAG5-6936 and by travel grants for thesis work at Kitt Peak National Observatory by NOAO. EE acknowledges support provided by the National Science Foundation grant AST 9617145. EJJ wishes to thank David Helfand for motivating and guiding the original construction of the IPC source catalog and Ben Oppenheimer for generating the original IPC source catalog used as the basis for this work. EJJ acknowledges support from NASA contract NAS8-38249 and grant NAC5-1656 at MIT. We gratefully acknowledge Dr. Harald Ebeling for a detailed criticism of the original manuscript which led to a significant revision of this research. This research has made use of the High Energy Astrophysics Science Archive Research Center (HEASARC) provided by the NASA-Goddard Space Flight Center, the Einstein Online (EINLINE) database and the NASA Astrophysics Data System (ADS) maintained at the Smithsonian Astrophysical Observatory, the NASA-IPAC Extragalactic Database (NED) operated by the Caltech Jet Propulsion Laboratory under contract with the National Aeronautics and Space Administration, and the SIMBAD database, operated at the Centre des Données Astronomiques, Strasbourg, France. The Digitized Sky Surveys were produced at the Space Telescope Science Institute under U.S. Government grant NAG W-2166. The images of these surveys are based on photographic data obtained using the Oschin Schmidt Telescope on Palomar Mountain and the UK Schmidt Telescope.

APPENDIX

A. APPENDIX: NOTES ON INDIVIDUAL SOURCES

In this appendix we provide additional detail for individual sources of interest. We describe objects excluded from our catalog under special circumstances, sources in the three subsamples which were judged not to be groups or clusters of galaxies, and clusters discovered by other research groups. Those clusters discovered in the imaging program of this work will be presented in full detail in Paper 2. To obtain unabsorbed flux from instrumental count rates (and convert between

different bandpasses used by different groups) we have assumed a power-law spectral energy distribution with photon index $\Gamma = 1.5$ ($\alpha = 0.5$), and used the WPIMMS software to calculate conversions, using the weighted average neutral hydrogen column density obtained from W3nH. We assume the same spectral energy distribution to perform K-corrections when calculating rest-frame X-ray luminosities. These notes are appended to illustrate the scrutiny to which potential cluster sources were subjected by this work.

A.1. Sources #324 & #962

Detected in the HFS subsample, these two clusters were originally found by the first installment of the EMSS (the Medium Survey #1, MSS1 hereafter, Maccacaro et al. 1982; Stocke et al. 1983) but were not members in the final EMSS Catalog, as noted in Gioia et al. (1990b), because some of the integration time was discarded due to a more conservative detection algorithm than was used for the MSS1. Thus, these two source fell below the 4σ detection limit of the EMSS. Why these sources are redetected here is not completely obvious but, since both are identified as clusters, we assume that it is due to their extended flux and have retained them in the catalog. Source #324 (R.A., Decl. (J2000) = $01^h29^m02^s06$, $+ 07^\circ40'54''.7$) is identified with a compact galaxy group known as Shakhbazian 41 and is of individual interest due to the significant signs of interaction among its brightest member galaxies. Source #962 lies at R.A., Decl. (J2000) = $04^h41^m41^s53$, $- 10^\circ56'47''.0$. A third new catalog source (#4402, R.A., Decl. (J2000) = $09^h41^m04^s84$, $+ 11^\circ36'31''.1$), while not a member of the HFS subsample, was also detected in MSS1, where it was identified as a star. However, this source is also in the vicinity of a small, nearby galaxy group cataloged recently by Ramella et al. (1997) within the CfA redshift survey sky area. In this paper we identify this source with this group because the current technique found it to be extended, although only new, sensitive X-ray observations can determine the true identity of source #4402. All three MSS1 sources have quite modest X-ray luminosities, consistent with being small groups or poor clusters of galaxies.

A.2. Source #420

Re-detected in the HFS subsample of our catalog, this distant cluster ($z = 0.833$, R.A., Decl. (J2000) = $01^h52^m43^s35$, $- 13^\circ58'01''.5$) has been rediscovered in the *ROSAT* PSPC database independently by three different groups (Rosati et al. 1998; Ebeling et al. 2000; Romer et al. 2000) and its reason for not being discovered in the EMSS has been discussed in detail by Ebeling et al. (2000). Briefly, Ebeling et al. argue that the asymmetric nature of the X-ray emission from this cluster caused the EMSS to mis-locate an accurate centroid and so underestimate the flux due to its asymmetric and somewhat low surface brightness nature. We have not obtained optical images for this cluster but the extent seen by *ROSAT* as well as the temperature and Fe line measured by *Beppo* SAX are ample reasons that the cluster ID is secure. It has $L_X = 8 \times 10^{44} h_{50}^{-2}$ ergs s^{-1} in the 0.5 – 2.0 keV band (Ebeling et al. 2000), which corresponds to $14.6 \times 10^{44} h_{50}^{-2}$ ergs s^{-1} in the 0.3 – 3.5 keV band, and an unabsorbed flux of 5.00×10^{-13} ergs $s^{-1} \text{ cm}^{-2}$. The first aperture IPC unabsorbed flux for this source is 3.61×10^{-13} ergs $s^{-1} \text{ cm}^{-2}$, but it increases to 6.9 and 10.5×10^{-13} ergs $s^{-1} \text{ cm}^{-2}$ in the second and third apertures, respectively. The X-ray contour maps of this cluster shown in Ebeling et al. indicate a spatial extent of at least 5 arcmin in diameter, suggesting that at least the flux in the 2nd aperture should be used. We therefore regard the luminosity value of Ebeling et al. as a lower limit, but we will adopt it instead of our own estimates because Ebeling et al. have performed a more detailed analysis of the newer available X-ray data.

A.3. Source #992

This field, part of the “ramp” subsample, has several identified galaxies from the nearby cluster Abell 516 at $z = 0.1407$, which has an optical center 7'.1 away from the X-ray source location, based on the SIMBAD coordinates. However, upon a more detailed investigation, we found that the study which obtained the optical galaxy redshifts (Ciardullo et al. 1985) notes that the optical cluster center appears to be in the vicinity of the two galaxies with measured redshifts and thus at the location of source #992. A visual inspection of the SIMBAD position for Abell 516 on the DSS finds no large concentration of galaxies and that the nearest concentration of galaxies is at the source #992 position. Therefore, we assign source #992 to Abell 516. Further, the target of the original IPC image in which this source was discovered is a supercluster which includes Abell 516. Therefore, source #992 is eliminated from the catalog as target related for the same reason as source #4359 in the random source subsample. Without the extensive analysis provided by the inclusion of this source in the non-random “ramp” sample, this source would have remained in the catalog as a viable serendipitous source (see §5.1).

A.4. Source #1757

A member of the random sample, this source exhibits a small concentration of galaxies in its color-magnitude diagram consistent with a group at $z \sim 0.35$, but the formal measured B_{gc} value is negative. A *ROSAT* All-Sky-Survey source lies 4.2 arcmin NNW of #1757 and so could only contribute flux to the third aperture. We conclude that this cluster is not rich enough and so would not be bright enough to have this source be identified as a cluster of galaxies. It is more likely a blend of sources.

A.5. Source #1767

A member of the HFS subsample, we initially identified this source as a cluster based on a large galaxy over-density, a good concentration in its color-magnitude diagram at $z \approx 0.4$, and a measured B_{gc} value of $\approx 1000 (h_{50}^{-1} \text{ Mpc})^{1.77}$. The

X-ray centroid lies at R.A., Decl. (J2000) = $10^h48^m28^s.84, + 06^\circ43'26''.8$. However, we found a RASS FSC detection lying within the 2nd IPC aperture, but $> 500 h_{50}^{-1}$ kpc away from the BCG of the apparent cluster. This source was positionally consistent with a prominent galaxy which is nearly a full magnitude brighter in B than two adjacent galaxies, though all three had similar R and V colors. The galaxy also appeared more centrally concentrated in B , suggesting it is an AGN. Combined with the fact that the FSC source was of equivalent X-ray flux to our measurement of the second IPC aperture flux, it seems very likely that this AGN contributes significantly to the X-ray detection. Even if the apparent cluster is as rich as measured, at best this field is a blend of sources, neither of which would be of sufficient individual flux to be added to the EMSS. This source only obtains a $S/N > 4.0$ in the third and fourth IPC apertures, further suggesting that is a blend.

A.6. Source #1772

Also a member of the HFS subsample, this field contains an apparent overdensity of galaxies. The X-ray centroid lies at R.A., Decl. (J2000) = $10^h49^m48^s.98, + 06^\circ44'53''.6$. However, we find that a large fraction are late-type galaxies, and that there are no clumps in color to indicate a significant galaxy overdensity (i.e., we find $B_{gc} \leq 250 \text{ Mpc}^{1.77}$, which is below Abell Richness Class 0) in any part of the image. Unfortunately, the exposures in one of our filters are not photometric for this field, and galaxy color measurements may be inaccurate. However, it seems to be an optical superposition of many field galaxies, with some possible poor groups as well. Therefore we do not identify this field as a cluster of galaxies.

A.7. Source #2036

Also a random sample source, this field has two apparently overlapping concentrations of galaxies. The first group has an estimated galaxy over-density of $B_{gc} \sim 50 - 200 (h_{50}^{-1} \text{ Mpc})^{1.77}$, at redshift $z \sim 0.35 - 0.45$ which suggests an X-ray luminosity of $L_X = 0.004 - 0.1 \times 10^{44} \text{ ergs s}^{-1}$ and an expected X-ray flux of $0.01 - 0.15 \times 10^{-13} \text{ ergs s}^{-1} \text{ cm}^{-2}$ (0.3 – 3.5 keV). The second group has an estimated galaxy over-density of $B_{gc} \sim 300 (h_{50}^{-1} \text{ Mpc})^{1.77}$, at redshift $z \sim 0.60$ which suggests an X-ray luminosity of $L_X = 0.3 \times 10^{44} \text{ ergs s}^{-1}$ and an expected X-ray flux of $0.12 \times 10^{-13} \text{ ergs s}^{-1} \text{ cm}^{-2}$ (0.3 – 3.5 keV). The observed first aperture flux of this source is $1.0 \times 10^{-13} \text{ ergs s}^{-1} \text{ cm}^{-2}$ (0.3 – 3.5 keV), significantly higher than even the combination of both possible groups. Additionally, no PSPC source was detected in the region of the X-ray centroid or the galaxy overdensity to a 3σ limit of $1 \times 10^{-13} \text{ ergs s}^{-1} \text{ cm}^{-2}$ (0.3 – 3.5 keV), although a 6σ PSPC source lies 4 arcmin to the south of #2036 (see Table 5) and could contribute flux to the third aperture detection of this source. We conclude that, while the ID of this source is not obvious, it is not a cluster of galaxies, but a blend of sources, similar to source #1757.

A.8. Source #2203

This is a $z = 0.39$ cluster identified in the SHARC (Romer et al. 2000) as RXJ1241.5+3250. Our X-ray centroid lies at R.A., Decl. (J2000) = $12^h41^m33^s.56, + 32^\circ49'50''.4$. Based on the provided *ROSAT* PSPC count rate of 0.04 cts s^{-1} in the 0.4 – 2.0 keV band (Romer et al. 2000) we calculate an unabsorbed flux of $4.66 \times 10^{-13} \text{ ergs s}^{-1} \text{ cm}^{-2}$ (0.4 – 2.0 keV), equivalent to $8.71 \times 10^{-13} \text{ ergs s}^{-1} \text{ cm}^{-2}$ in the 0.3 – 3.5 keV band. The unabsorbed fluxes of 8.52 and $11.8 \times 10^{-13} \text{ ergs s}^{-1} \text{ cm}^{-2}$ in the 2nd and 3rd IPC apertures, respectively, are consistent with the SHARC estimates, and confirm their cluster ID. We adopt the redshift and X-ray luminosity values from their work.

A.9. Source #2407

Another HFS subsample member, this field contains an apparent optical overdensity of galaxies. The X-ray centroid lies at R.A., Decl. (J2000) = $13^h19^m36^s.59, + 55^\circ06'35''.6$. However, under detailed scrutiny we find only two small physical concentrations. The first clump to the NNE is at a redshift of $z \sim 0.20 - 0.25$, with galaxy overdensity of $B_{gc} \approx 210 (h_{50}^{-1} \text{ Mpc})^{1.77}$, and an approximate luminosity of only $L_X = 9 \times 10^{42} \text{ ergs s}^{-1}$, corresponding to $f_X = 1.8 \times 10^{-14} \text{ ergs s}^{-1} \text{ cm}^{-2}$. The second clump to the South is at a redshift of $z \sim 0.35 - 0.40$, with galaxy overdensity of $B_{gc} \approx 250 (h_{50}^{-1} \text{ Mpc})^{1.77}$, and thus $L_X = 1.5 \times 10^{43} \text{ ergs s}^{-1}$, corresponding to $f_X = 1.3 \times 10^{-14} \text{ ergs s}^{-1} \text{ cm}^{-2}$. The smallest IPC aperture detection corresponds to $4 \times 10^{-13} \text{ ergs cm}^{-2} \text{ s}^{-1}$, easily greater than the sum of these sources. We must assume that an as yet unidentified AGN in the field is the bulk of our IPC detection. Therefore, we do not identify this source as a cluster of galaxies.

A.10. Source #2616

This source is identified as an extended X-ray source by Vikhlinin et al. (1998a). However, they cannot make an optical confirmation of a cluster due to a nearby bright star obscuring the field. Our X-ray centroid lies at R.A., Decl. (J2000) = $14^h15^m40^s.29, + 19^\circ06'00''.5$. We leave this field unidentified.

A.11. Source #2626

This is a $z = 0.138$ cluster identified in the SHARC (Romer et al. 2000) as RXJ1416.4+2315. Our X-ray centroid lies at R.A., Decl. (J2000) = $14^h16^m27^s.35, + 23^\circ15'24''.6$. Based on the provided *ROSAT* PSPC count rate of 0.112 cts s^{-1} in the 0.4 – 2.0 keV band (Romer et al. 2000) we calculate an unabsorbed flux of $13.3 \times 10^{-13} \text{ ergs s}^{-1} \text{ cm}^{-2}$ (0.4 – 2.0 keV), equivalent to $24.8 \times 10^{-13} \text{ ergs s}^{-1} \text{ cm}^{-2}$ in the 0.3 – 3.5 keV band. The unabsorbed fluxes of $10.9, 19.9, \& 38.8 \times 10^{-13} \text{ ergs s}^{-1} \text{ cm}^{-2}$ in the 2nd, 3rd, & 4th IPC apertures, respectively, are consistent with the SHARC estimates, and confirm their cluster ID. We adopt the redshift and X-ray luminosity values from their work.

A.12. *Source #2937*

This field may contain a loosely concentrated poor group at low redshift ($z < 0.10$), judging by the appearance of nearby galaxies in the field. Our X-ray centroid lies at R.A., Decl. (J2000) = $15^h36^m02^s20, +23^\circ18'34''.3$. The low X-ray luminosity of such a group makes it unlikely to be the dominant X-ray emitter in this field, if it is a physical association of galaxies at all. We can only state that this is not a rich cluster of galaxies, and that we do not as yet identify an obvious optical counterpart to the X-ray emission.

A.13. *Source #3065*

This field contains an apparent distant cluster $6'$ SW of the field center in a deep R image. Our X-ray centroid lies at R.A., Decl. (J2000) = $16^h08^m53^s06, +28^\circ53'31''.3$. Unfortunately, we do not have the multi-color data necessary to estimate its redshift and richness. However, because the cluster is so far from the X-ray centroid, we consider it likely that this field contains a blend of sources, and the cluster only contributes to the 3rd and 4th aperture detections, which exhibit a dramatic increase in S/N compared to the second aperture. Therefore we do not identify this source as a cluster of galaxies, but leave it unidentified pending more observations.

A.14. *Source #3175*

This field is identified as J164154.2+4000033, a $z = 1.005$ QSO found by Crampton et al. (1992). Vikhlinin et al. (1998a) identify this source as a cluster of galaxies at $z = 0.44 - 0.55$. It seems likely that this field appears as a blend of sources to the IPC, and so we do not add it to our cluster list.

A.15. *Source #3469*

This source is identified by Vikhlinin et al. (1998a) as a portion of Abell S840 ($z = 0.0152$). We concur and add it to our cluster identifications. Our X-ray centroid lies at R.A., Decl. (J2000) = $20^h03^m28^s38, -55^\circ56'44''.8$. Based on their provided flux of 4.76×10^{-13} ergs s^{-1} cm^{-2} (0.5 – 2.0 keV), we adopt a luminosity of $L_X = 41.95 \times 10^{44} h_{50}^{-2}$ ergs s^{-1} in the 0.3 – 3.5 keV band.

A.16. *Source #4057*

This field, which is part of the random sample, exhibited no obvious galaxy overdensity and so was not evaluated for cluster richness. Our X-ray centroid lies at R.A., Decl. (J2000) = $02^h39^m51^s80, -23^\circ20'42''.8$. Our optical imaging indicates only a very weak galaxy overdensity at best. However, this source is identified as a $z = 0.42 - 0.53$ cluster by Vikhlinin et al. (1998a), although they do not have spectroscopic confirmation. The *ROSAT* extrapolated total flux (including absorption by galactic hydrogen) for the purported cluster is given by Vikhlinin et al. as $8.4 \pm 1.8 \times 10^{-14}$ ergs s^{-1} cm^{-2} in the 0.5 – 2.0 keV bandpass. From the IPC data, we estimate the absorbed flux in the same bandpass to be 1.1 and 2.4×10^{-13} ergs s^{-1} cm^{-2} in the first and third apertures, respectively. The S/N rises from 3.5 to 4.4 between these same apertures, so source #4057 enters the catalog due to its third aperture flux. However, the PSPC observation also detected a point source with flux $1 - 2 \times 10^{-13}$ ergs s^{-1} cm^{-2} 3.3 arcmin from the IPC source location, and thus contributing substantially to the third aperture flux. Therefore, we identify source #4057 as a combination of sources and so do not identify the possible cluster of galaxies of Vikhlinin et al. as responsible for the entry in our catalog.

A.17. *Source #4746*

This field is apparently an optical superposition of galaxies with no discernible concentration in redshift. Our X-ray centroid lies at R.A., Decl. (J2000) = $13^h34^m03^s27, -08^\circ26'14''.4$. The most significant structure in the color-magnitude diagram lies at approximately $z \sim 0.13 - 0.17$, but our range of estimates for the B_{gc} value includes zero. This may be a very poor group, but it is not responsible for the X-ray emission detected in this field, which is likely to be a blend of sources. We note that Vikhlinin et al. (1998a) identify this field as an extended X-ray source, and a “likely false” cluster of galaxies, because it did not appear as a cluster in their optical imaging. We also do not identify this source as a cluster of galaxies.

REFERENCES

- Adami, C., Ulmer, M. P., Romer, A. K., Nichol, R. C., Holden, B. P., & Pildis, R. A. 2000, *ApJS*, 131, 391
Bahcall, N. A. & Fan, X. 1998, *ApJ*, 504, 1
Ciardullo, R., Ford, H., & Harms, R. 1985, *ApJ*, 293, 69
Couteau, P. & Gili, R. 1994, *A&AS*, 106, 377
Crampton, D., Cowley, A. P., Hartwick, F. D. A., & Ko, P. W. 1992, *AJ*, 104, 1706
de Grandi, S., Böhringer, H., Guzzo, L., Molendi, S., Chincarini, G., Collins, C., Cruddace, R., Neumann, D., Schindler, S., Schuecker, P., & Voges, W. 1999, *ApJ*, 514, 148
Della Ceca, R., Scaramella, R., Gioia, I. M., Rosati, P., Fiore, F., & Squires, G. 2000, *A&A*, 353, 498
Dickey, J. M. & Lockman, F. J. 1990, *ARA&A*, 28, 215
Donahue, M., Mack, J., Scharf, C., Lee, P., Postman, M., Rosati, P., Dickinson, M., Voit, G. M., & Stocke, J. T. 2001, *ApJ*, 552, L93
Donahue, M., Stocke, J. T., & Gioia, I. M. 1992, *ApJ*, 385, 49
Donahue, M. & Voit, G. M. 1999, *ApJ*, 523, L137
Donahue, M., Voit, G. M., Gioia, I., Lupino, G., Hughes, J. P., & Stocke, J. T. 1998, *ApJ*, 502, 550
Donahue, M., Voit, G. M., Scharf, C. A., Gioia, I. M., Mullis, C. R., Hughes, J. P., & Stocke, J. T. 1999, *ApJ*, 527, 525
Dressel, L. L. & Condon, J. J. 1976, *ApJS*, 31, 187
Ebeling, H., Edge, A. C., Fabian, A. C., Allen, S. W., Crawford, C. S., & Böhringer, H. 1997, *ApJ*, 479, L101
Ebeling, H., Edge, A. C., & Henry, J. P. 2001, *ApJ*, 553, 668

- Ebeling, H., Jones, L. R., Perlman, E., Scharf, C., Horner, D., Wegner, G., Malkan, M., Fairley, B. W., & Mullis, C. R. 2000, *ApJ*, 534, 133
- Ebeling, H., Voges, W., Böhringer, H., Edge, A. C., Huchra, J. P., & Briel, U. G. 1996, *MNRAS*, 281, 799
- Edge, A. C. & Stewart, G. C. 1991, *MNRAS*, 252, 428
- Edge, A. C., Stewart, G. C., Fabian, A. C., & Arnaud, K. A. 1990, *MNRAS*, 245, 559
- Eke, V. R., Cole, S., & Frenk, C. S. 1996, *MNRAS*, 282, 263
- Ellingson, E., Lin, H., Yee, H. K. C., & Carlberg, R. G. 2001, *ApJ*, 547, 609
- Evrard, A. E. & Henry, J. P. 1991, *ApJ*, 383, 95
- Giacconi, R., Branduardi, G., Briel, U., Epstein, A., Fabricant, D., Feigelson, E., Holt, S. S., Becker, R. H., Boldt, E. A., & Serlemitsos, P. J. 1979, *ApJ*, 230, 540
- Gioia, I. M., Henry, J. P., Maccacaro, T., Morris, S. L., Stocke, J. T., & Wolter, A. 1990a, *ApJ*, 356, L35
- Gioia, I. M., Henry, J. P., Mullis, C. R., Voges, W., Briel, U. G., Böhringer, H., & Huchra, J. P. 2001, *ApJ*, 553, L105
- Gioia, I. M. & Luppino, G. A. 1994, *ApJS*, 94, 583
- Gioia, I. M., Maccacaro, T., Schild, R. E., Wolter, A., Stocke, J. T., Morris, S. L., & Henry, J. P. 1990b, *ApJS*, 72, 567
- Giommi, P., Tagliaferri, G., Beuermann, K., Branduardi-Raymont, G., Brissenden, R., Graser, U., Mason, K. O., Mittaz, J. D. P., Murdin, P., Pooley, G., Thomas, H., & Tuohy, I. 1991, *ApJ*, 378, 77
- Gladders, M. D. & Yee, H. K. C. 2000, *AJ*, 120, 2148
- Gregory, P. C. & Condon, J. J. 1991, *ApJS*, 75, 1011
- Griffith, M. R., Wright, A. E., Burke, B. F., & Ekers, R. D. 1995, *ApJS*, 97, 347
- Gunn, J. E., Hoessel, J. G., & Oke, J. B. 1986, *ApJ*, 306, 30
- Hamilton, T. T. & Helfand, D. J. 1987, *ApJ*, 318, 93
- . 1993, *ApJ*, 418, 55
- Hamilton, T. T., Helfand, D. J., & Wu, X. 1991, *ApJ*, 379, 576
- Harris, D. E., Forman, W., Gioia, I. M., Hale, J. A., Harnden, F. R., Jones, C., Karakashian, T., Maccacaro, T., McSweeney, J. D., Primini, F. A., Schwarz, J., Tananbaum, H. D., & Thurman, J. 1990, "The Einstein Observatory Catalog of IPC X-ray Sources" (Cambridge, Mass.: Smithsonian Institution, Astrophysical Observatory, January 1990, edited by Harris, D.E.)
- Harvanek, M., Ellingson, E., Stocke, J. T., & Rhee, G. 2001, *AJ*, submitted
- Henry, J. P. 1997, *ApJ*, 489, L1
- . 2000, *ApJ*, 534, 565
- Henry, J. P., Gioia, I. M., Maccacaro, T., Morris, S. L., Stocke, J. T., & Wolter, A. 1992, *ApJ*, 386, 408, (H92)
- Hewett, P. C., Foltz, C. B., & Chaffee, F. H. 1995, *AJ*, 109, 1498
- Hewitt, A. & Burbidge, G. 1987, *ApJS*, 63, 1
- Hogg, D. W. 1999, unpublished, astro-ph/9905116 v3
- Jones, C. & Forman, W. 1999, *ApJ*, 511, 65
- Kaiser, N. 1991, *ApJ*, 383, 104
- Kodama, T. & Arimoto, N. 1997, *A&A*, 320, 41
- Kodama, T., Arimoto, N., Barger, A. J., & Arag'ón-Salamanca, A. 1998, *A&A*, 334, 99
- Lewis, A. D. 2001, Ph.D Thesis, University of Colorado at Boulder
- Lewis, A. D., Ellingson, E., Morris, S. L., & Carlberg, R. G. 1999, *ApJ*, 517, 587
- Lewis, A. D., Ellingson, E., & Stocke, J. T. 2001, *ApJ*, accepted (Paper 2)
- Lewis, A. D. & Stocke, J. T. 2001, in preparation (Paper 3)
- Maccacaro, T., Gioia, I. M., Zamorani, G., Feigelson, E. D., Fener, M., Giacconi, R., Griffiths, R. E., Murray, S. S., Stocke, J., & Liebert, J. 1982, *ApJ*, 253, 504
- Moran, E. C., Helfand, D. J., Becker, R. H., & White, R. L. 1996, *ApJ*, 461, 127
- Morris, S. L., Hutchings, J. B., Carlberg, R. G., Yee, H. K. C., Ellingson, E., Balogh, M. L., Abraham, R. G., & Smecker-Hane, T. A. 1998, *ApJ*, 507, 84
- Moscardini, L., Matarrese, S., De Grandi, S., & Lucchin, F. 2000, *MNRAS*, 314, 647
- Moshir, M. E. A. 1990, in *IRAS Faint Source Catalogue*, version 2.0 (1990)
- Mulchaey, J. S. & Zabludoff, A. I. 1998, *ApJ*, 496, 73
- Olsen, E. H. 1994, *A&AS*, 106, 257
- Oppenheimer, B. R., Helfand, D. J., & Gaidos, E. J. 1997, *AJ*, 113, 2134, (OHG97)
- Perlman, E. S., Horner, D. J., Jones, L. R., Scharf, C. A., Ebeling, H., Wegner, G., & Malkan, M. 2000, *ApJS*, submitted
- Pesce, J. E., Fabian, A. C., Edge, A. C., & Johnstone, R. M. 1990, *MNRAS*, 244, 58
- Ramella, M., Pisani, A., & Geller, M. J. 1997, *AJ*, 113, 483
- Rector, T. A., Stocke, J. T., & Perlman, E. S. 1999, *ApJ*, 516, 145
- Romer, A. K., Nichol, R. C., Holden, B. P., Ulmer, M. P., Pildis, R. A., Merrelli, A. J., Adami, C., Burke, D. J., Collins, C. A., Metevier, A. J., Kron, R. G., & Commons, K. 2000, *ApJS*, 126, 209
- Rosati, P., della Ceca, R., Burg, R., Norman, C., & Giacconi, R. 1995, *ApJ*, 445, L11
- Rosati, P., della Ceca, R., Norman, C., & Giacconi, R. 1998, *ApJ*, 492, L21
- Scharf, C. A., Jones, L. R., Ebeling, H., Perlman, E., Malkan, M., & Wegner, G. 1997, *ApJ*, 477, 79
- Stocke, J. T., Liebert, J., Gioia, I. M., Maccacaro, T., Griffiths, R. E., Danziger, I. J., Kunth, D., & Lub, J. 1983, *ApJ*, 273, 458
- Stocke, J. T., Morris, S. L., Gioia, I. M., Maccacaro, T., Schild, R., Wolter, A., Fleming, T. A., & Henry, J. P. 1991, *ApJS*, 76, 813
- Truemper, J. 1993, *Science*, 260, 1769
- Vikhlinin, A., McNamara, B. R., Forman, W., Jones, C., Quintana, H., & Hornstrup, A. 1998a, *ApJ*, 502, 558
- . 1998b, *ApJ*, 498, L21
- Voit, G. M. 2000, *ApJ*, 543, 113
- Yee, H. K. C. 1991, *PASP*, 103, 396
- Yee, H. K. C. & López-Cruz, O. 1999, *AJ*, 117, 1985
- Zabludoff, A. I. & Mulchaey, J. S. 1998, *ApJ*, 496, 39

TABLE 3
NEW SOURCES IN THE RANDOMLY-SELECTED SUBSET OF 133 EMSS IPC FIELDS

Cat. #	RA J2000	Dec. J2000	Seq.	$c.r._1^a$	$c.r._2^a$	$c.r._3^a$	σ_1^b	σ_2^b	σ_3^b	Eval. ^c
64	00 25 52.52	+ 17 17 30.2	1810	4	10	16	3.74	4.52	5.09	X
69	00 26 47.83	+ 17 22 59.9	1810	3	5	19	3.02	2.78	4.47	X
71	00 27 35.88	+ 17 06 25.7	1810	5	11	31	3.53	3.71	6.29	X
97	00 38 37.56	+ 29 32 05.3	7917	3	7	21	2.92	2.71	4.39	C
3886	00 41 53.22	- 01 39 40.0	5393	6	11	15	4.42	4.80	4.90	X
3909	00 48 05.59	- 25 24 43.0	2082	5	7	14	3.82	3.84	4.27	X
3915	00 52 33.50	+ 01 48 37.3	8455	4	8	13	3.56	4.10	4.04	X
161	00 53 10.38	+ 01 52 25.3	8455	4	8	15	3.18	3.23	4.70	C:
163	00 53 18.24	+ 01 39 20.6	8455	5	6	16	4.11	3.73	5.17	X
5341	01 10 29.63	+ 39 17 02.0	8464	5	7	0	4.50	4.14	0	X
288	01 21 33.29	- 03 28 43.4	7208	4	8	13	3.17	3.55	4.53	...
298	01 23 04.75	- 03 21 59.7	7208	4	7	14	3.18	3.51	4.80	X
302	01 23 33.74	- 03 46 29.7	7208	4	14	29	2.71	4.28	5.72	X
299	01 23 37.36	- 03 36 55.0	7208	4	6	12	3.35	2.99	4.24	X
353	01 37 19.54	- 04 50 08.5	863	12	17	41	3.05	3.22	4.58	X
451	02 06 33.49	- 37 37 33.4	5388	5	11	23	3.29	3.25	4.55	...
446	02 06 37.13	+ 23 30 48.5	852	5	7	14	3.74	4.40	5.29	X
450	02 06 56.27	- 37 59 07.6	5388	9	14	23	3.80	4.15	4.86	...
4040	02 24 32.49	+ 07 06 45.9	3256	0	6	23	0	3.23	4.96	X
4057	02 39 51.80	- 23 20 42.8	2014	7	0	16	3.51	0	4.41	X
657	03 20 05.65	- 43 10 47.7	3105	8	9	29	3.26	3.03	4.08	X
804	03 58 55.38	+ 10 19 44.3	6311	4	7	16	3.12	3.53	4.97	X
807	04 00 16.33	- 36 33 16.3	4577	0	13	31	0	3.07	5.07	...
1415	08 26 10.41	+ 26 43 12.9	5929	0	0	12	0	0	4.27	X
1417	08 26 14.37	+ 10 45 44.3	5125	0	9	25	0	2.76	4.70	X
1424	08 27 23.02	+ 26 37 15.3	5929	3	7	12	3.83	4.36	5.14	X
4359 ^d	08 28 41.60	+ 65 43 12.1	305	4	6	19	3.34	2.82	4.94	C ^d
4374	08 47 06.81	+ 18 34 10.4	4059	0	0	31	0	0	4.60	X
1477	08 47 10.46	+ 18 20 22.8	4059	7	0	23	3.04	0	4.02	X
4375	08 52 16.54	+ 28 27 33.8	5504	2	4	10	2.97	3.61	4.54	X
1568	09 23 24.81	+ 34 20 31.1	2101	4	5	18	3.11	2.93	4.46	X
1584	09 29 31.23	+ 06 24 27.9	10382	4	6	18	4.42	3.63	5.72	X
1587	09 29 33.22	+ 06 04 25.0	10382	2	4	12	2.74	2.84	4.41	X
1757	10 44 26.87	+ 06 32 15.6	6344	8	16	21	3.27	3.89	4.75	X
4508	11 41 40.31	+ 34 08 57.0	3530	0	10	26	0	2.62	4.65	...
1918	11 47 16.73	+ 00 33 32.5	7712	9	15	22	3.33	3.94	4.80	...
4524	11 48 23.85	+ 00 43 01.4	7712	5	9	17	3.05	3.33	4.63	...
1955	11 58 55.30	+ 32 23 00.4	443	20	34	42	3.34	4.23	4.78	X
1975	12 07 41.02	- 29 49 18.0	5801	4	0	16	3.55	0	4.34	...
2026	12 17 41.99	+ 28 02 53.1	7036	0	0	15	0	0	5.13	X
2036	12 18 47.38	+ 28 10 51.0	7036	3	5	16	3.13	2.69	4.72	X
2282	12 55 01.06	+ 11 29 33.8	4037	9	23	33	2.65	3.20	4.58	X
2392	13 17 16.82	+ 58 05 28.6	6879	0	0	19	0	0	4.51	...
2437	13 30 36.79	+ 24 54 02.3	498	6	13	23	4.02	4.81	5.64	X
2450	13 31 17.59	+ 25 15 29.9	498	6	9	25	3.37	4.21	5.15	...
4740	13 31 28.42	+ 25 00 59.4	498	7	9	9	3.88	4.14	3.77	...
2483	13 37 10.32	+ 03 49 46.3	5547	2	5	12	3.04	3.14	4.19	...
4759	13 37 21.63	+ 03 28 06.2	5547	3	6	14	3.04	3.39	4.88	...
2517	13 49 46.76	- 03 49 10.9	4261	9	12	24	4.33	4.52	4.74	...
2657	14 23 57.80	- 18 36 07.4	3454	0	8	18	0	2.53	4.29	...
2658	14 24 08.69	- 18 20 08.5	3454	7	14	23	3.37	2.91	4.22	...
4845	14 44 31.57	+ 51 54 55.9	6317	3	6	18	2.98	2.97	4.83	X
2748	14 48 26.28	- 16 26 27.2	3989	11	21	28	3.37	4.06	3.89	...

TABLE 3—*Continued*

Cat. #	RA J2000	Dec. J2000	Seq.	$c.r._1^a$	$c.r._2^a$	$c.r._3^a$	σ_1^b	σ_2^b	σ_3^b	Eval. ^c
2799	15 04 52.79	− 33 08 13.1	6407	7	16	30	2.72	3.62	4.55	...
2858	15 17 41.03	+ 22 44 24.8	8047	0	0	35	0	0	4.45	...
4917	15 33 40.36	+ 31 27 40.5	7642	5	8	12	2.82	2.95	4.69	...
2923	15 33 56.47	+ 31 17 33.2	7642	6	7	27	3.40	3.68	5.17	X
2919	15 34 18.93	+ 01 45 27.6	5708	4	0	29	2.60	0	4.53	...
2933	15 35 27.41	+ 01 46 07.7	5708	9	14	18	3.80	4.78	4.91	...
2971	15 48 54.63	+ 02 23 50.6	5397	5	10	24	3.09	2.91	4.42	...
2989	15 53 07.64	− 04 26 09.0	2911	5	7	15	3.10	2.87	4.11	...
5101	18 05 58.21	+ 67 51 45.7	8780	0	0	17	0	0	4.61	X
3439	18 53 01.06	+ 59 20 28.2	4946	11	10	35	3.92	3.35	4.20	...
3564	21 36 17.10	+ 00 59 14.3	7801	8	11	19	4.42	3.57	4.54	X
5173	21 44 17.47	+ 14 58 46.7	7605	0	4	12	0	2.78	4.52	...
5187	22 01 40.94	− 56 46 28.4	5652	5	7	22	3.15	2.53	4.28	X
5188	22 02 06.59	− 56 37 04.1	5652	0	0	33	0	0	5.98	...
5192	22 04 18.62	− 56 40 10.4	5652	0	0	20	0	0	5.00	X
5208	22 53 51.98	− 17 21 35.4	2074	12	19	33	3.78	4.23	3.60	X
3739	23 14 31.50	− 42 32 24.9	5259	13	16	58	3.20	3.44	5.71	X
3741	23 14 57.19	− 42 39 23.3	5259	0	0	45	0	0	4.82	...
5223	23 17 01.45	− 42 07 27.3	7582	17	33	49	4.00	4.36	5.07	X
3752	23 19 30.71	− 36 04 13.2	7569	19	28	34	4.21	5.40	5.03	...
3765	23 28 07.20	− 29 59 04.5	4499	12	26	35	3.04	3.15	4.26	...

^aCount rates in the 0.3 – 3.5 keV band, given in 10^{-3} sec^{-1} .

^bAn entry of zero indicates a value less than the detection threshold limit of 2.5.

^cIdentification of the source based on all the data in Tables 4, 5, & 6: C is a cluster of galaxies; X is not a cluster of galaxies; C: is a possible cluster of galaxies; if there is no entry, no definitive determination is possible at this time.

^dSource was removed from the Random Subsample, see §3.2, and entry in Table 4.

TABLE 4
IDENTIFICATIONS OR COUNTERPARTS FOR RANDOM SUBSAMPLE SOURCES

Cat. #	ID or Counterpart	Eval. ^a	References
64	Radio: NVSS 002349.97 +171717; 17 mJy		
97	Radio: 87GB 00352.2+291502		1
	Galaxy Group: NGC 0181/0183/0184 ($z = 0.018$)	C	2
163	QSO: 0050+0123 ($z = 1.439$)	A	3
299	Star: PPM 183386 ($V = 10.0$)	S	
	Radio: PMN J0123-0348		4
1955	AGN: EXO 1156.3+3239 ($z = 0.215$)	A	5
2282	Star: HD 112221 (GV, $V = 9.10$, B-V=0.45)	S	6
4359 ^b	Galaxy Group related to A665 ($z = 0.20$)	C	7
5101	Star: SAO 17771 (K2 $V=9.3$ B-V=1.4)	S	
5187	IRAS: 21586-5652; probable AGN	A	8
5208	Star: EXO 2251.1-1737 ($V=16$)	S	5
5223	QSO: HB89 2314-423 ($z = 0.27$)	A	9
5341	Star: Gliese 1416 K2 double ($V = 9.8$, B-V = 1.2)	S	10

^aIdentification of the source based on the information available: C is a cluster of galaxies; A is an AGN; S is a star.

^bSource was removed from the Random Subsample, due to being target related; see §3.2.

References. — (1) Gregory & Condon (1991); (2) Dressel & Condon (1976); (3) Hewett et al. (1995); (4) Griffith et al. (1995); (5) Giommi et al. (1991); (6) Olsen (1994); (7) this paper; (8) Moshir (1990); (9) Hewitt & Burbidge (1987); (10) Couteau & Gili (1994)

TABLE 5
OTHER X-RAY DETECTIONS OF RANDOM SUBSAMPLE SOURCES

Cat #	Satellite/ Detector ^a	% ^b	Δ^c [arcmin]	3σ Limit ^d	Extent?	Comments	Eval. ^e
64	R-H	$\geq 50\%$	0.7		No	Point Source Contributes	
69	R-H	$\sim 100\%$	4.0	1.9	No		X
71	R-H	30-60%	0.9		No	Point Source Contributes	
163	R-H	$\geq 60\%$	0.7		No	QSO ID	X
446	R-P	30-200%	0.9		No	Variable Source	X
657	R-H, R-P	$\leq 50\%$	4.8	2.1	No		X
804	R-H	$\leq 50\%$	1.7	1.0	No		
1415	R-P	$\leq 30\%$	1.2		No	PSPC Source Contributes	
1424	R-P	$\sim 100\%$	0.8		No	Other PSPC source nearby	X
1477	R-P	$\leq 50\%$	0.3		?		
1757	R-R	$\leq 30\%$	4.2		No	RASS Source Contributes to 3rd aperture flux	
1918	R-P	$\sim 50\%$	0.5		?		
1955	R-H	$\sim 100\%$	0.6		No	Two other HRI sources within 1'	X
2036	R-P	$\sim 100\%$	4.0	1.0	?	Contributes to 3rd aperture flux	X
2437	R-P	$\sim 100\%$	0.7		No		X
2923	R-P	$\sim 200\%$	0.9		No	Point Source	X
2933	R-P	$\sim 100\%$	1.9	6.0	?	Short PSPC exposure	
2989	R-P	$\geq 100\%$	0.4		?		
3564	R-P	$\sim 100\%$	1.0		No	2nd PSPC Source 1'.3 away	X
3739	R-H, R-P	80-150%	0.5		No	Variable Source	X
3741	R-H, R-P	10-30%	2.5	1.8	No	Variable Source	P
3909	R-H, R-P	$\sim 50\%$	1.2		No	Point Source	X
4057	R-P	$\sim 50\%$	3.3	1.0	No	Point Source	X
4374	R-P	$\leq 50\%$	1.8	1.4	?		
4508	R-P	$\sim 50\%$	0.5		?		
4845	R-P	$\geq 50\%$	1.3	0.9	?		
5187	R-H, R-P R-R	200-400%	0.5		No	Variable Source: ID=QSO	X
5192	R-P	$\sim 20\%$	4.1	0.7	No		X
5208	R-P, E	$\sim 100\%$	0.6		No	ID=M8 Star	X
5223	R-P	80-100%	0.3		No	Variable Source: ID=QSO	X

^aR-H is *ROSAT* HRI, R-P is *ROSAT* PSPC, R-R is RASS, E is *EXOSAT/CMA*.

^bEstimated percentage of the IPC flux detected in the other dataset.

^cAngular offset between the positions of the source reported in this catalog and the source in the other dataset in arcmin.

^d 3σ flux limit within the 2'.5 diameter IPC detect aperture, in units of 10^{-13} ergs s^{-1} cm^{-2} , where no source was detected in the first aperture.

^eEvaluation of the source based on the available X-ray data alone: X is not a cluster of galaxies; C is a cluster of galaxies; P indicates that a point source contributes significantly to the detected flux, but does not account for the entire source. No entry in this column means that a definitive determination of source identification is not possible based upon the X-ray data available.

TABLE 6
OPTICAL IMAGING OF SOURCES FROM THE RANDOM SAMPLE

Cat. #	Comments	Eval. ^a
64	Cirrus	X
69		X
71		X
97	Galaxy Group, NGC 181/183/184 ($z = 0.018$)	C
161	Possible cluster; $B_{gc} = 610 - 2230 (h_{50}^{-1} \text{ Mpc})^{1.77}$; $z = 0.52 - 0.59$ Second structure $B_{gc} = 370 - 1610 (h_{50}^{-1} \text{ Mpc})^{1.77}$; $z = 0.25 - 0.49$	C:
298		X
302		X
353		X
446	Bright Star	X
804		X
1415		X
1417		X
1477		X
1568		X
1584		X
1587		X
1757	Small group at $z \sim 0.35$, but measured $B_{gc} < 0$	X
1955	<i>EXOSAT</i> QSO ($z = .215$)	X
2026		X
2036	Likely blend of 2 high- z groups which have too low a B_{gc} value to account for the detection	X
3886		X
3915	PHL Object; likely AGN	X
4040		X
4057		X
4374		X
4375		X
4845		X
5341	Bright Star	X

^aEvaluation of the source; letter designations are the same as in Table 3

TABLE 7
X-RAY DATA FOR SOURCES FROM THE RAMP SUBSAMPLE

Cat. #	RA J2000	Dec. J2000	Seq.	$c.r._1^a$	$c.r._2^a$	$c.r._3^a$	σ_1	σ_2	σ_3
623	03 07 24.71	+ 17 17 35.2	6830	4	7	12	4.36	4.38	5.56
641	03 15 04.12	+ 14 37 55.0	3954	5	5	9	5.22	5.15	3.47
793	03 52 05.28	+ 24 40 49.0	3175	24	33	45	4.23	4.41	5.16
795	03 53 35.05	+ 25 36 22.3	7408	10	16	28	4.19	4.18	4.60
992	04 49 39.30	- 08 47 16.1	3748	6	12	15	3.42	4.14	4.87
1033	05 04 30.95	- 11 51 52.1	10225	4	8	17	4.14	4.29	6.11
1310	07 16 39.58	+ 37 19 27.8	3554	7	9	25	2.87	2.79	4.01
1328	07 38 31.78	+ 65 24 08.3	589	4	9	18	2.66	3.26	4.91
1342	07 47 12.51	+ 38 48 11.8	3148	6	14	28	2.88	3.42	4.62
1350	07 56 23.86	+ 39 02 04.6	2622	11	12	37	3.46	2.95	4.18
1492	08 51 40.06	+ 33 31 23.3	3921	23	34	41	3.25	3.68	4.22
1605	09 39 58.76	- 02 49 26.6	7427	7	15	13	3.64	4.69	4.22
4045	02 35 04.04	- 03 40 44.5	7922	5	11	16	3.32	4.02	4.49

^aCount rates are given in 10^{-3} sec^{-1} .

Note. — A few sources (e.g., #641) only increase their S/N in the 4th aperture (data not shown), thereby allowing them to be included in the “Ramp” subsample.

TABLE 8
SUMMARY OF IMAGING AND DATABASE SEARCH FOR SOURCES FROM THE RAMP SUBSAMPLE

Cat. #	Comments	Eval. ^a
623		X
641	2 bright stars > 4' offset	X
793	Variable PSPC sources account for 100% of flux ID=K5 star	X
795	V=6.3 mag star 4'6 N could contribute to 3rd aperture flux	X
992	Abell cluster 516 ($z=0.141$)	C
1033		X
1310	$B_{gc} = 790 - 1410 (h_{50}^{-1} \text{ Mpc})^{1.77}$; $z = 0.34 - 0.40$	C
1328	<i>ROSAT</i> PSPC source contributes 20% of flux in 2nd aperture	X
1342	Bright star and FIRST radio source at 1' offset	X
1350	several FIRST radio sources at < 1'; no significant galaxy overdensity	X
1492	$B_{gc} = 1550 - 2920 (h_{50}^{-1} \text{ Mpc})^{1.77}$; $z = 0.42 - 0.50$ pair of BCGs and a blue arc RASS FSC detection 52''S of galaxy overdensity <i>ROSAT</i> source flux consistent with cluster ID	C
1605	$B_{gc} = 670 - 1050 (h_{50}^{-1} \text{ Mpc})^{1.77}$; $z \approx 0.22 - 0.27$	C
4045	Unresolved <i>ROSAT</i> X-ray source 0'6 offset accounts for 100% of flux	X

^aLetter designations are the same as in Table 3.

TABLE 9
X-RAY DATA FOR SOURCES OBSERVED IN THE HIGH FLUX AND S/N SUBSAMPLE

Cat. #	RA J2000	Dec. J2000	Seq.	$c.r._1^a$	$c.r._2^a$	$c.r._3^a$	σ_1^b	σ_2^b	σ_3^b
1641	09 53 07.80	+ 07 33 36.6	5934	7	19	21	4.13	6.08	6.14
1681	10 07 51.41	+ 12 45 43.6	563	6	9	10	4.52	5.12	3.79
1767	10 48 28.84	+ 06 43 26.8	9049	9	23	38	2.57	2.88	4.75
1772	10 49 48.98	+ 06 44 53.6	9049	12	24	46	3.58	4.48	5.41
2128	12 31 56.36	+ 62 35 32.8	6869	8	12	25	4.46	5.09	5.96
2407	13 19 36.59	+ 55 06 35.6	4603	12	32	36	2.66	3.19	4.13
2436	13 30 11.38	+ 30 43 51.3	491	9	14	21	4.52	5.66	6.91
2465	13 35 10.41	+ 17 13 50.6	5376	15	33	39	3.97	5.44	5.87
2727	14 42 08.18	+ 28 36 28.3	237	15	29	39	3.89	4.17	4.38
2844	15 12 27.90	+ 72 00 47.6	6891	6	7	0	5.66	4.65	0
2906	15 31 55.38	+ 24 20 42.9	3121	15	19	19	4.86	5.06	4.69
2937	15 36 02.20	+ 23 18 34.3	10464	2	11	15	2.88	4.79	6.40
3065	16 08 53.06	+ 28 53 31.3	5719	6	9	19	3.56	4.53	5.95
3068	16 10 07.13	+ 19 05 43.3	3040	0	25	33	0	3.05	4.64
3244	17 08 12.15	+ 54 43 48.1	7663	8	24	29	3.43	3.98	5.01
3299	17 29 35.78	+ 52 30 46.1	3812	20	37	55	3.43	4.35	5.23
3353	17 55 51.73	+ 67 53 44.9	8757	0	25	60	0	2.81	4.54
4725	13 19 16.19	- 12 23 16.6	10244	9	17	19	3.28	4.73	5.65
4746	13 34 03.27	- 08 26 14.4	917	6	10	16	3.77	4.84	5.44
5064	17 18 33.36	+ 17 49 21.4	7481	5	10	15	3.31	5.11	3.36

^aCount rates are given in 10^{-3} sec^{-1} .

^bAn entry of zero indicates a value less than 2.5.

TABLE 10
SUMMARY OF IMAGING AND DATABASE SEARCH FOR SOURCES FROM THE HIGH FLUX AND S/N SUBSAMPLE

Cat. #	Comments	ID ^a
1641		X
1681	Cluster $z = 0.35 - 0.45$; $B_{gc} = 180 - 1030 (h_{50}^{-1} \text{ Mpc})^{1.77}$	C
1767	Cluster at $z = 0.37 - 0.45$; $B_{gc} = 880 - 1260 (h_{50}^{-1} \text{ Mpc})^{1.77}$ RASS FSC detection coincides with blue galaxy near IPC X-ray centroid <i>ROSAT</i> source flux matches 2nd IPC aperture flux Galaxy overdensity is in 3rd IPC aperture, likely blend with AGN	X
1772	Likely superposition of field galaxies; possible poor groups	X
2128		X
2407	2 poor groups likely a blend with unidentified X-ray sources	X
2436	Cluster $z = 0.22 - 0.28$; $B_{gc} = 1120 - 1680 (h_{50}^{-1} \text{ Mpc})^{1.77}$ possible 2nd cluster 5' NE, $z \sim 0.30$; $B_{gc} = 400 - 650 (h_{50}^{-1} \text{ Mpc})^{1.77}$	C
2465		X
2727		X
2844	Possible cluster $z = 0.33 - 0.44$; $B_{gc} = 640 - 1260 (h_{50}^{-1} \text{ Mpc})^{1.77}$ RASS FSC detection at location of galaxy overdensity <i>ROSAT</i> source flux is consistent with cluster ID	C:
2906	Possible cluster $z = 0.42 - 0.53$; $B_{gc} = 390 - 1410 (h_{50}^{-1} \text{ Mpc})^{1.77}$	C:
2937	Possible poor group at $z < 0.1$; insufficient richness to account for the X-ray source	X
3065	Possible blend of cluster 6' SW and unidentified sources	X
3068		X
3244		X
3299		X
3353	Definite $z < 0.1$ group RASS BSC detection just South of brightest E galaxy <i>ROSAT</i> source is extended, flux consistent with group ID	C
4725		X
4746	Optical superposition of galaxies	X
5064		X

^aEvaluation of the source; letter designations are the same as in Table 3

TABLE 11
NEW CLUSTERS IN THE EMSS

Cat. #	z	B_{gc}^a	$\log L_X^b$ from IPC	$\log L_X^b$ from B_{gc}	Sample	Notes	Ref.
97*	0.018	...	42.0 ± 0.1	...	Random	NGC 181/183 /184 Group	(1) (2)
161 [†]	0.52 – 0.59	610 – 2230	44.7 – 45.0	45.5	Random	Possible Cluster 2nd Cluster in Field	(1) (2)
324	0.085	...	43.5 ± 0.1	...	HFS	Shakbazian 41; found in MSS1	(3)
420	0.833	...	45.0 – 45.6	45.2 ^c	HFS	Found by <i>ROSAT</i> PSPC	(4)
962	0.152	...	43.9 ± 0.1	...	HFS	Found in MSS1	(3)
1310*	0.34 – 0.40	790 – 1410	44.5 – 44.9	45.3	Ramp		(2)
1492*	0.42 – 0.50	1550 – 2910	44.9 – 45.3	46.2 ^d	Ramp HFS		(2)
1605	0.22 – 0.27	670 – 1050	43.9 – 44.2	44.8	Ramp HFS		(2)
1681	0.35 – 0.45	180 – 1030	44.1 – 44.6	44.4	HFS		(2)
2203	0.39	...	44.8 – 45.0	44.8 ^c	HFS		(6)
2436	0.22 – 0.28	1120 – 1680	44.1 – 44.4	45.6	HFS	GHO Cluster 2nd Cluster in Field	(2) (5)
2626	0.138	...	44.1 – 44.3	44.3 ^c	HFS		(6)
2844 [†]	0.33 – 0.44	640 – 1260	44.3 – 44.8	44.8	HFS	Possible Cluster	(2)
2906 [†]	0.42 – 0.53	390 – 1410	44.6 – 45.0	45.0	HFS	Possible Cluster	(2)
3353	< 0.1	...	< 44.0	...	HFS		(2)
3469	0.0152	...	42.2 ± 0.1	41.9 ^c	...	Abell S840	(7)
4402	0.022	...	41.9 – 42.0	...	HFS	CfaN Group #54; found in MSS1	(3) (8)

Note. — Clusters denoted with a * fell below the revised S/N limits described in §5.1. Clusters denoted with a [†] are possible cluster identifications, pending further investigation.

^aGalaxy over-density in units of $(h_{50}^{-1} \text{ Mpc})^{1.77}$.

^bLog of the cluster X-ray luminosity in the 0.3 – 3.5 keV band in $h_{50}^{-2} \text{ ergs s}^{-1}$. IPC luminosity is calculated from the third aperture count rate, see § 4.4; the range of values includes an estimate of the Poisson error on the detected count rate. For luminosity estimates based on B_{gc} -values, see § 3.3.

^cLuminosity is taken from the Reference indicated in Column (8), converted to the 0.3 – 3.5 keV band, see entry in Appendix A.

^dThis luminosity is likely too high to be physical; the $B_{gc} - L_X$ relationship we use here may be suspect above $B_{gc} \sim 1500 (h_{50}^{-1} \text{ Mpc})^{1.77}$.

References. — (1) This Paper; (2) Lewis et al. (2001); (3) Stocke et al. (1983); (4) Ebeling et al. (2000); (5) Gunn et al. (1986); (6) Perlman et al. (2000); Romer et al. (2000); (7) Vikhlinin et al. (1998a); (8) Ramella et al. (1997)

TABLE 12
THE REVISED EMSS XLF DATA

Redshift Shell z	Log L_X (0.3 – 3.5 keV) [ergs s^{-1}] Luminosity Bins					
	43.7 – 44.0	44.0 – 44.3	44.3 – 44.6	44.6 – 44.9	44.9 – 45.2	45.2 – 45.5
	Number of Clusters in each Bin					
0.14 – 0.20	2	4	5	5
	3	4	5	5
	3.8	4	5	5
0.20 – 0.30	2	8	6	4	...	1
	2.3	9.3	6.3	4	...	1
	2.6 – 3.6	10.3 – 14.2	6.6 – 7.6	4	...	1
0.30 – 0.60	...	4	5	7	4	...
	...	4.4	5.9	8.9	4.3	1
	...	4.7 – 5.9	6.6 – 9.2	10.3 – 12.0	4.5 – 4.9	1
0.60 – 0.85	1	1	...
	1	2	...
	1	2.8	...

Note. — The first entry in each bin is the original H92 value modified to reflect the updates for newer work described in §5.2. The second entry in each bin reflects the number of clusters resulting from the addition of just those 7.5 new clusters found thus far in our identification work from Table 11. The third entry is the value resulting from the addition of the estimated 13.1 – 24.9 clusters projected by this work to be missing from the entire EMSS sky area (including the extrapolation at the upper end of the range for clusters not yet found in the HFS sample; see § 5.2). Note that we have added a new redshift bin to accommodate the new high- z clusters now observed.